Structures of Photosynthetic Reaction Centers With Alternative Cofactors

by

Amelia Hardjasa

B.Sc., The University of British Columbia, 2010
B.A., The University of British Columbia, 2010

A THESIS SUBMITTED IN PARTIAL FULFILLMENT OF
THE REQUIREMENTS FOR THE DEGREE OF

MASTER OF SCIENCE

in

The Faculty of Graduate and Postdoctorate Studies

(Microbiology and Immunology)

THE UNIVERSITY OF BRITISH COLUMBIA

(Vancouver)

July 2015

Abstract

Rhodobacter sphaeroides is a model organism for the study of bacterial photosynthesis. The *R. sphaeroides* photosynthetic reaction centre (RC) is the primary site of electron transfer, which is mediated by the photosynthetic pigments bacteriochlorophyll *a* (BChl) and bacteriopheophytin (BPhe). The substitution of key amino acid residues can change the type of cofactors present in the RC. In particular, studies have shown that when the leucine residue in position 214 of the M subunit [(M)L214] is converted into a histidine, the BPhe normally present in the neighbouring position (H_A) is replaced with a BChl.

This study investigated the hypothesis that steric exclusion by the coordinating residue causes dechelation of the central magnesium ion in BChl, producing BPhe. Crystal structures of RCs where (M)L214 is substituted for glycine and alanine were determined, which demonstrated that the presence of BPhe in the H_A pocket is unchanged despite decreasing the size of the residue in position (M)214. A crystal structure of an RC where (M)L214 is substituted for asparagine was also determined and showed that the replacement of BPhe with BChl at H_A occurs if residue (M)214 includes an amide moiety.

In the *R. sphaeroides* Δ*bchd* strain, which lacks the ability to make BChl, it is believed that the RC cofactor sites are populated exclusively with zinc-bacteriochlorophyll (Zn-BChl). The crystal structures of this Zn-BChl containing RC (Zn-RC) and a Zn-RC with the (M)L214H substitution (Zn-β-RC) were solved for the first time. These structures confirmed the presence of Zn-BChl in every cofactor position and the tetracoordination of the H_A Zn-BChl in the Zn-β-RC, as well as revealing that the occupancy of the H_B cofactor was much lower than that of all other cofactors.

Preface

The majority of the work presented in this thesis is drawn from published literature. This work was made possible by extensive collaboration with Dr. J Thomas Beatty's laboratory at the University of British Columbia. Since the collaboration provides crucial support for the findings, portions from the publications have been incorporated into this thesis. Below are detailed the contributions of my collaborators.

Saer, R.G., Hardjasa, A., Rosell, F.I., Mauk, A.G., Murphy, M.E.P., and Beatty, J.T. (2013) The role of Rhodobacter sphaeroides photosynthetic reaction center residue M214 in the composition, absorbance properties, and conformations of H_A and B_A cofactors. Biochemistry, ***52****(13), 2206-2217.* I performed the crystallization, data collection, and structure solution and analysis, and wrote the first draft of the relevant sections of the manuscript. R. Saer performed the purification, spectroscopy, and photosynthetic growth studies, and drafted all other sections of the manuscript. Drs. M. Murphy and J. Beatty edited the manuscript. The text and figures in the Materials and Methods, Results, and Discussion sections of this manuscript were adapted and included in the corresponding sections of this thesis.

Saer, R.G., Pan, J., Hardjasa, A., Lin, S., Rosell, F., Mauk, A.G., Woodbury, N.W., Murphy, M.E.P., and Beatty, J.T. (2014) Structural and kinetic properties of Rhodobacter sphaeroides photosynthetic reaction centers containing exclusively Zn-coordinated bacteriochlorophyll as bacteriochlorin cofactors. BBA Bioenergetics, ***1837****(3), 366-374.* I performed the crystallization, data collection, and some of the structure solution. M. Murphy performed the remainder of the structure solution and analysis, and wrote the

text in the corresponding sections of the manuscript. A. Chan created Figure 2 of the manuscript. R. Saer performed the purification and spectroscopy, and drafted all other sections of the manuscript. Drs. M. Murphy and J. Beatty edited the manuscript. Only the sections of this manuscript related to data I produced were adapted and included in the corresponding sections of this thesis.

The work in this thesis was approved by the University of British Columbia Biosafety Committee under the project title "Heme and Iron Uptake in Pathogenic Bacteria", Certificate #B130096.

Table of Contents

List of Tables

List of Figures

Acknowledgements

I acknowledge the financial support for this work provided by a CIHR Canada Graduate Scholarship. I also thank the Stanford Synchrotron Research Laboratory and the Canadian Light Source for synchrotron data collection.

I am deeply indebted to my supervisor, Dr. Michael Murphy, for his immense and unflagging support, guidance, and understanding. This thesis would not have been possible without his continual and generous efforts on my behalf. Under his supervision I have had unprecedented opportunities to grow both as a scientist and human being, all of which have been invaluable.

I am also very grateful to Dr. Tom Beatty for his advice and support over several years. It was his guidance that first set me on the path to becoming a scientist. I would like to thank my primary collaborator in the Beatty Lab, Dr. Rafael Saer, for his scientific direction and contribution to the work published in this thesis.

I would also like to thank all of the other members of the Murphy Lab and Beatty Lab who have supported me on my way: Paul Jaschke, Angele Arrieta, Anson Chan, Jason Grigg, Stephanie Pfaffen, Catherine Gaudin, Daniel Jun, Jeanette Beatty, my students Jaimie and Fabian, and many others, all of whom have been not only trusted friends and supports but also exemplary role models.

I am immeasurably grateful to Darlene Birkenhead for her support and encouragement, without which this work would not have been completed.

Finally, I am deeply thankful to all of my friends and family for their forbearance and goodwill over the course of my graduate studies. Especially, I would like to thank Ivan Zverev for his continual kindness, reassurance, and patience through all the ups and downs of this chapter of my life.

Chapter 1

Introduction

1.1 Bacterial photosynthesis

Sunlight is one of the most freely available and bountiful energy sources on earth. Photosynthesis gives organisms the means whereby this abundant energy can be accessed for growth, and is thus responsible for a vast portion of primary production, being the main metabolic mode for all plants, algae, cyanobacteria, and many other organisms. One well known group of prokaryotic photosynthesizers is the purple photosynthetic bacteria. These bacteria only perform photosynthesis under anoxic conditions, especially those with an abundance of hydrogen sulfide [46]. They are thus prolific in the depths of aquatic environments including lakes, ponds, and lagoons. The oxygenic phototrophs that live above the purple bacteria absorb most of the short-wavelength, high-energy incoming light with their chlorophylls [16]. Purple bacteria consequently have developed specialized pigment-protein complexes which preferentially absorb light at 750 nm and above, resulting in the purple colour from which they derive their name [64].

The subject of this study, *Rhodobacter sphaeroides*, is a well-studied member of the purple photosynthetic bacteria, as it possesses many features that make it ideal for experimentation. It exhibits extraordinary metabolic diversity, including phototrophy and heterotrophy, as well as being relatively amenable to laboratory culture and genetic manipulation [31]. Although light energy can be scanty at the depths where *R. sphaeroides* is found, the species is nonetheless is able to thrive, thanks in large part to the high quantum efficiency of its photosynthetic reaction center (RC) and light harvesting complexes; nearly 100 % of absorbed photons are converted into usable energy in the form

of a proton motive force [73].

1.2 Characteristics of *R. sphaeroides*

1.2.1 Photosynthesis *in vivo*

Upon exposure to light and anaerobic or microaerophilic conditions, invaginations form in the *R. sphaeroides* cellular membrane known as chromatophores or intracytoplasmic membranes (ICMs), which for the most part bud incompletely from the cellular membrane, although it is possible for them to exist as free-floating vesicles [25]. These ICMs are enriched with photosynthetic apparatus proteins, and their presence has the effect of increasing membrane surface area available for light capture without requiring a drastic jump in cell volume [18]. In the ICM, the photosynthetic reaction center complex can be found surrounded by light harvesting antenna complexes (light harvesting complex 1 (LH1) and 2 (LH2)), which assist in transferring captured photons to the reaction center, but are not a requirement for photosynthetic growth [37, 68].

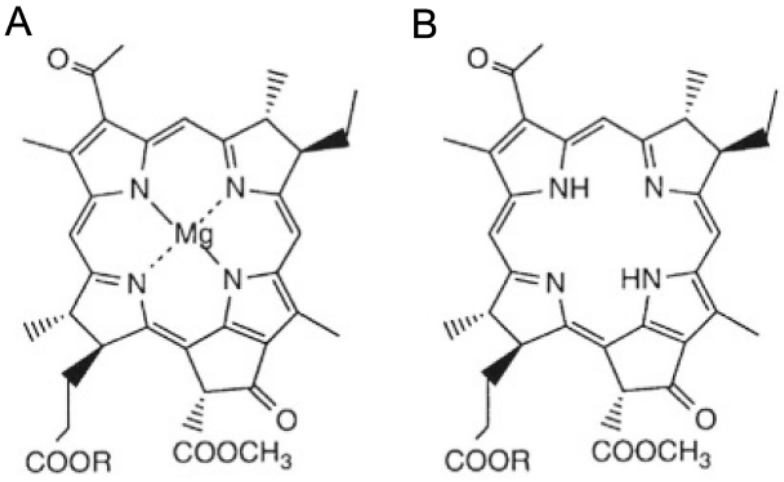

Figure 1.1: Structural formulae of BChl (A) and BPhe (B), with R representing the cofactor tail (usually phytyl). Reprinted from [64] with permission.

1.2.2 Cofactors

The role of the reaction center is the conversion of trapped light energy to a transmembrane proton gradient via electron transfer through the protein. This is mediated by a set of porphyrin-derived cofactors, sometimes referred to as "chlorins" or "pigments", terms which will be used interchangeably throughout this text. The two cofactor types found natively in the *R. sphaeroides* reaction center are bacteriochlorophyll *a* (BChl) and bacteriopheophytin (BPhe) (Figure 1.1).

Biosynthesis. BChl is derived from protoporphyrin-IX through the well-elucidated bacteriochlorophyll biosynthetic pathway (Figure 1.2). Firstly, the enzymes encoded by the *bch* operon genes *bchHDI* catalyze the chelation of a central magnesium ion by the pyrrole ring. After several subsequent reductions of the porphyrin, the final step is the addition of a hydrophobic "tail" by means of an esterifying alcohol [9]. BPhe is identical to BChl structurally, except for the lack of the central ion. It is believed that BPhe is derived from BChl by the removal of the Mg^{2+} [2], although it has not yet been determined whether a specific "magnesium dechelatase" protein exists to perform this role, or whether some other means is responsible for removal of the central ion, such as the environment of the cofactor in the reaction center itself.

Hydrophobic tails. Little is known about the role of the hydrophobic tails in various chlorins. In *R. sphaeroides*, the esterifying alcohol is phytol, resulting in a phytyl tail. Although most BChls and many chlorophylls (Chl) incorporate a phytyl tail, this is not universal; for instance, BChls in *Rhodospirillum rubrum* have tails esterified by the less saturated geranylgeraniol (Figure 1.3) [40].

In 1999, Addlesee and Hunter identified the protein responsible for reduction of the esterifying alcohol prior to its attachment to the main BChl macrocycle [1]. It is believed that a mutation in this gene is responsible for the variation in the *R. rubrum* tail [2]. A

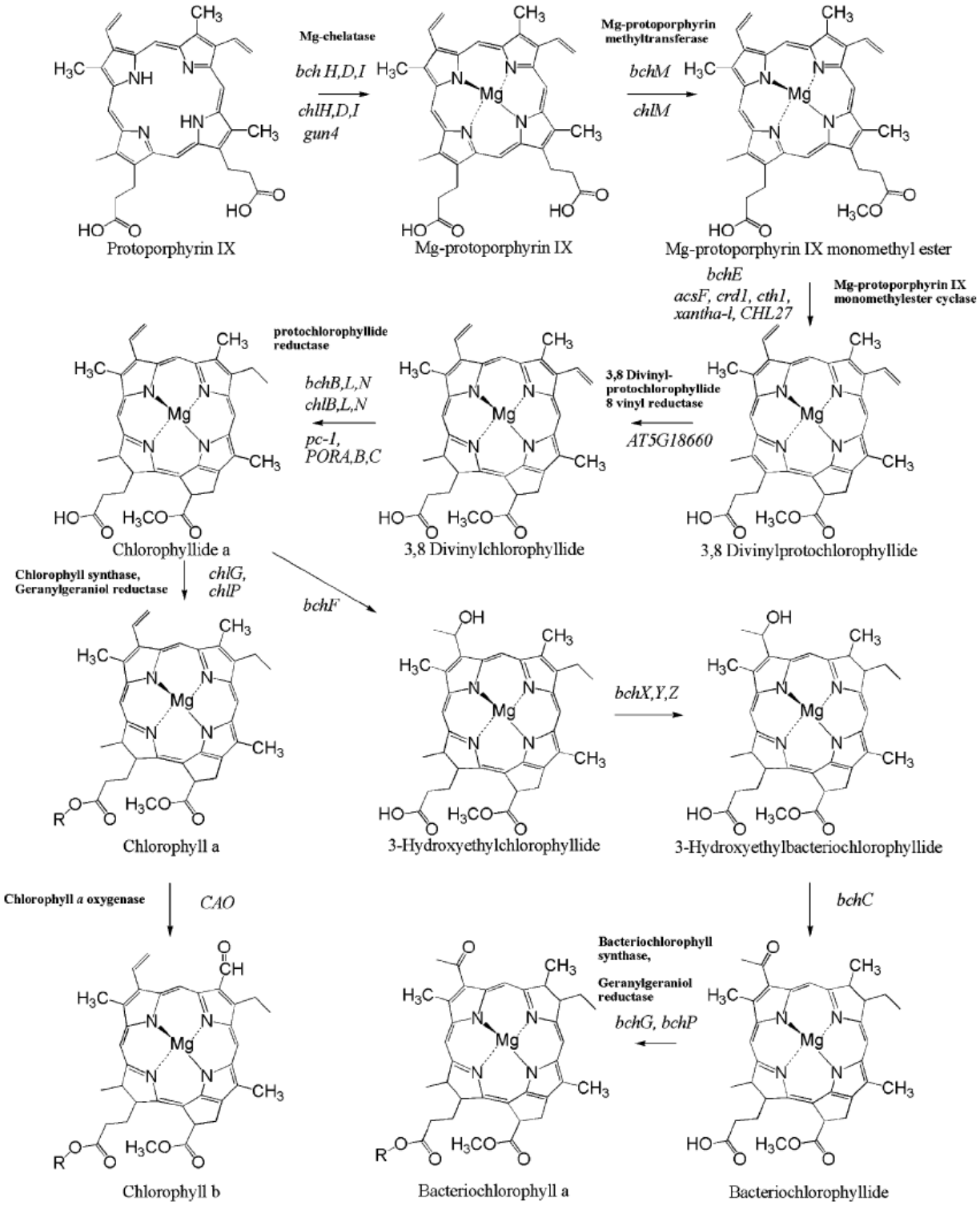

Figure 1.2: Biosynthetic pathway of BChl and chlorophyll *a* from protoporphyrin-IX. Reprinted from [9] with permission.

transposon mutant of *R. sphaeroides* lacking this reductase was able to grow photosynthetically, although it had much lower levels of light harvesting complexes and an overall lower growth rate. The reaction center was not specifically investigated, however, so it is unknown whether electron transfer in the RC was impaired or whether the lack of LH2 was solely responsible for the reduction in growth [10]. Wen *et al.* also investigated the effects of removing the reductase in the green bacterium *Chloroflexus aurianticus* [72]. Their study focused on the FMO complex, a trimeric complex containing 7 BChls per monomer that mediates electron transfer from the light harvesting complex to the *C. aurianticus* RC. Similarly, they found that overall amounts of FMO protein had decreased, but they also noted that there was more pigment heterogeneity in the FMO proteins containing the altered BChls.

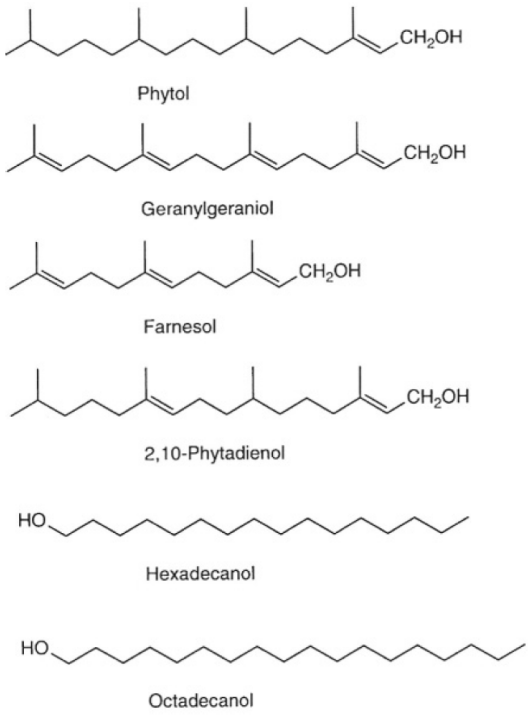

Figure 1.3: Different types of esterifying alcohols found attached to BChl and BPhe as tails in photosynthetic bacteria. *R. sphaeroides* cofactors have exclusively phytyl tails, but geranylgeranyl tails are found in, *e.g.*, *Rhodospirillum rubrum*. Reprinted from [64] with permission.

1.3 The *R. sphaeroides* RC

1.3.1 History of purification and X-ray crystallography

Purification. One large benefit of *R. sphaeroides*' diverse metabolism is its ability to grow in the dark heterotrophically. Otherwise, modifications that resulted in impaired photosynthetic growth might be outcompeted by the wild type bacterium when grown photosynthetically. In combination with the development of a simple method for obtaining large quantities of relatively pure RC protein by Goldsmith and Boxer in 1996 [26], this has led to the dominance of *R. sphaeroides* as the organism of choice for studying bacterial photosynthetic reaction centers. Hence, the following structural details will focus on the *R. sphaeroides* RC, although differences from reaction centers of other studied purple phototrophic bacteria will be noted when relevant.

Crystallization. The bacterial photosynthetic reaction center has the distinction of being the first membrane protein to have its structure determined by X-ray crystallography in 1985, for which the authors later received the Nobel Prize in Chemistry [17]. Although the first such structure determined was of the *Blastochloris viridis* (formerly *Rhodopseudomonas viridis*) RC, subsequent study focused on the *R. sphaeroides* RC thanks to its aforementioned greater utility in laboratory research. Since then, it has been studied extensively, with almost a hundred structures deposited in the Protein Data Bank (PDB). Despite this, only few high-resolution wild type structures are available, with only one structure determined to greater than 2.0 Å resolution (PDB entry 2J8C, 1.8 Å).

The first crystallization of the *R. sphaeroides* RC by Allen was in somewhat complicated conditions derived from those used for *R. viridis*. The protein solution contained

RC at a concentration of 5.5 mg/ml, 0.1 % LDAO, 2.5 % 1,2,3-heptanetriol, 3 % triethylammonium phosphate, 1.2 M $(NH_4)_2SO_4$, 10 mM Tris HCl (pH 8.0), 0.6 mM EDTA, and 0.1 % NaN_3, over a reservoir of 2.1 M $(NH_4)_2SO_4$, and crystals took 2-9 weeks to appear [4]. The dark-coloured crystals grew in monoclinic (*P2*) and orthorhombic (*C222*) space groups and were photosynthetically active, as demonstrated by spectroscopy. This first structure was solved to a resolution of 3.5 Å. As purification techniques have improved, the complexity of required crystallization conditions has decreased correspondingly, typically requiring only a potassium phosphate buffer (1.0-1.8 M), the amphiphile 1,2,3-heptanetriol (1.5 - 5 % weight by volume, depending on detergent concentration), and a solubilizing detergent. The RC has also served as a fertile testing ground for techniques specific to membrane protein crystallization, being among the first proteins crystallized by lipidic cubic and lipidic sponge phase methods [39]. These techniques use the lipid monoolein to form porous lipidic structures containing the protein, which facilitates crystallization, possibly by enhancing the long-term stability of the molecules [34].

Organization of the RC. The RC comprises three subunits titled L, M, and H 1.4. The H subunit is a globular protein primarily located on the cytoplasmic side, with a single transmembrane α-helix near the amino terminus. In contrast, the L and M subunits each contain five transmembrane helices, which are the major transmembrane portion of the RC. The L and M subunits form an approximately symmetrical complex (the LM complex) around a rotational axis, with abundant contact between the two proteins. On the periplasmic side, there are five helical segments in each subunit lying approximately perpendicular to the transmembrane helices; in the cytoplasm, the LM complex contacts the H subunit. The transmembrane region of the LM complex forms a cage-like structure around eight electronically active cofactors and an Fe^{2+} ion.

The cofactors comprise six chlorins and two ubiquinone-10s, divided along two nearly

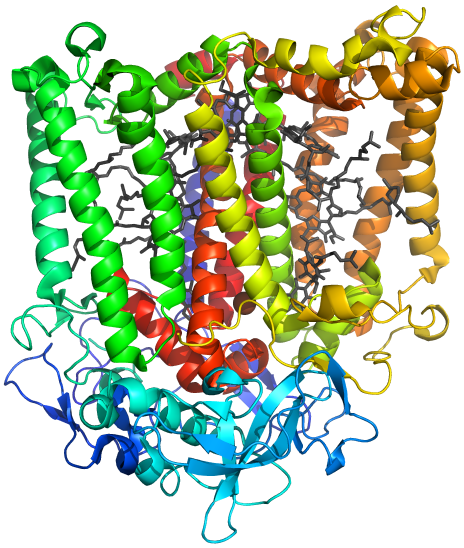

Figure 1.4: Three-dimensional structure of the *R. sphaeroides* RC, from PDB entry 2J8C. The globular H subunit, which is situated in the cytoplasm, is shown in blue. The L and M subunits, coloured green and yellow respectively, form the major transmembrane portion of the protein complex with five transmembrane helices each. These helices surround the electronically active cofactors, shown in grey.

symmetrical branches termed the A and B branches. In the native reaction center, electron transfer occurs only through the A branch.

The first cofactor site holds two closely associated BChls, known as the special pair. Below the special pair sit two accessory BChls, one on each branch, which are in turn adjacent to one BPhe each. Finally, a ubiquinone can be found below each BPhe, with the non-heme iron between them. These four paired sets, and their positions, are referred to as the P, B, H, and Q sites respectively. A subscript A or B denotes in which branch the cofactor is situated (see Figure 1.5).

Structural characterization. The first RC structures confirmed many predictions on the nature of the complex, such as its situation in the membrane and the special pair comprising two abutting BChls [5, 14, 52, 78]. Structures of the RC with cytochrome c_2 bound have shown its presence on the periplasmic side, congruent with its role in

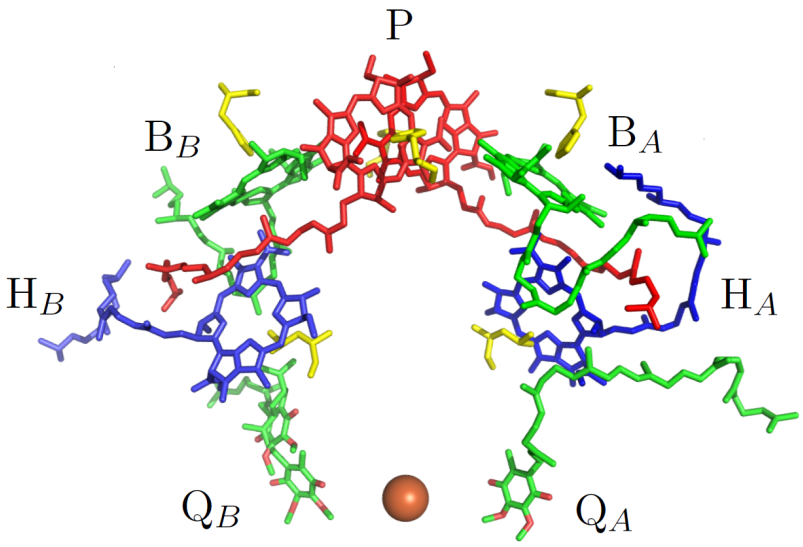

Figure 1.5: Arrangement of cofactors in the wild type *R. sphaeroides* reaction center. The cofactors are approximately symmetrical, with two branches labeled A and B. Electron transfer only occurs down branch A in the native RC. Bacteriochlorins are found at three sites: P, the special pair BChl; B, the accessory BChl; and H, the BPhe. Site Q is occupied by quinones and a structural non-heme iron is located between the two branches.

regenerating the special pair to neutral state [6]. Another surprising discovery that was not suggested by spectroscopic data was the presence of a bilateral cofactor pathway, symmetrical to a r.m.s.d of 0.7 Å in the special pair; this was shortly followed by the observation that, although both sets of cofactors are present, only one of the branches is active in electron transfer[5]. The locations of the centers of the chlorin rings were well-conserved as compared to the previously characterized RC of *R. viridis*[3]. Curiously, although early reports indicated considerable conformational variation in the phytyl tails of B_A and B_B, more recent structures have exhibited no such difference [5, 14, 20]. It is possible that the poorer resolution of these older structures resulted in the mistaken assignation of electron density to a tail instead of a detergent molecule.

Lipids and detergents. Purification and crystallization of the reaction center, as with most membrane proteins, involves the solubilization of the protein in detergent. Through

neutron-scattering experiments, Roth *et al.* examined RC crystals and found that the solubilizing detergent, either LDAO or BOG, formed elliptical micelles around the hydrophobic transmembrane regions of the protein, as well as facilitating crystal contacts between multiple copies of the RC [59]. The majority of these detergent molecules were not ordered and thus not visible in the X-ray structures. Although for the most part these detergent arrangements are similar to what would be expected in a lipid bilayer, any given detergent molecule in the crystal structure may not be representative of the reaction center *in vivo*.

Several studies have noted the presence of native (*i.e.*, not present in the crystallization or solubilization media) lipid molecules on the surface of the RC, most frequently cardiolipin (CDL), the glycolipid glucosylgalactosyl diacylglycerol (GGD), and the lipid phosphatidylcholine (PC), although the orientations and positions of these lipids do not always appear to be consistent between structures [13, 36, 48]. For example, in earlier structures the density for the three tails of cardiolipin had been modeled with three LDAO molecules, as the density was often weak and/or discontinuous. However, McAuley *et al.* showed in 1999 that continuous density could be fit for this lipid; furthermore, additional site-directed mutagenesis experiments observed that disrupting the putative binding sites for this lipid resulted in decreased RC stability [24, 48]. It is possible that other regions currently modeled by detergent molecules suffer similarly from misinterpreted electron density and that more such lipids may be found. The use of brominated lipids has shown some promise in this direction [58].

1.3.2 Catalytic cycle of the RC

The kinetics of electron transfer in the RC have been studied intensively over the past few decades [49, 55, 56, 73, 76, 77] and are briefly summarized below. Currently, the generally understood sequence of events is as follows: The catalytic cycle of the RC is

initiated when the absorption of a photon excites the special pair P, with the excited state referred to as P*. Subsequently, P* decays via the transfer of an electron to the neighbouring B_A cofactor, giving rise to the $P^+B_A^-$ state, with a time constant estimated at approximately 3 ps. From this point, it is possible for backwards charge recombination to occur, returning $P^+B_A^-$ to the neutral, unexcited ground state. However, in the wild type reaction center the rate of this reaction is almost negligible. Instead, the electron is passed on to H_A, forming $P^+H_A^-$, in less than 1 ps, then to Q_A in about 200 ps. Q_A^- then reduces Q_B, producing ubisemiquinone. The oxidized P^+ meanwhile receives an electron from a cytochrome c_2 to return it to the P state. This transfer pattern occurs once more, with the second reduction of Q_B producing a quinol, QH_2. QH_2 leaves the Q_B site and diffuses through the membrane; meanwhile the Q_B site is refilled with an oxidized quinone, completing the acceptor quinone cycle. The quinol is oxidized by the cytochrome bc_1 complex, which results in the release of two protons into the periplasm. Cytochrome c_2 accepts one electron from the cytochrome bc_1 complex and can therefore serve as an electron donor to P^+. This coupling of electron flow to proton translocation creates a proton motive force which can eventually be used by an ATP synthase. This cycle is extremely efficient, with virtually every captured photon contributing successfully to electron transfer.

1.3.3 Spectroscopic characteristics of the RC

Investigation of the electronic characteristics of the *R. sphaeroides* RC can be performed using absorption spectroscopy, with greater detail visible at lower temperatures [63, 76]. The conjugated ring systems of the chlorin-derived cofactors in the reaction center give rise to two prominent absorption peaks, one along each axis, termed the Q_x and Q_y transitions. Q_x transition peaks can be found in the 500-700 nm region, while Q_y transition peaks are found in the 700-900 nm range. In the wild type reaction center, peaks are associated with the cofactors as seen in Figure 1.6 below.

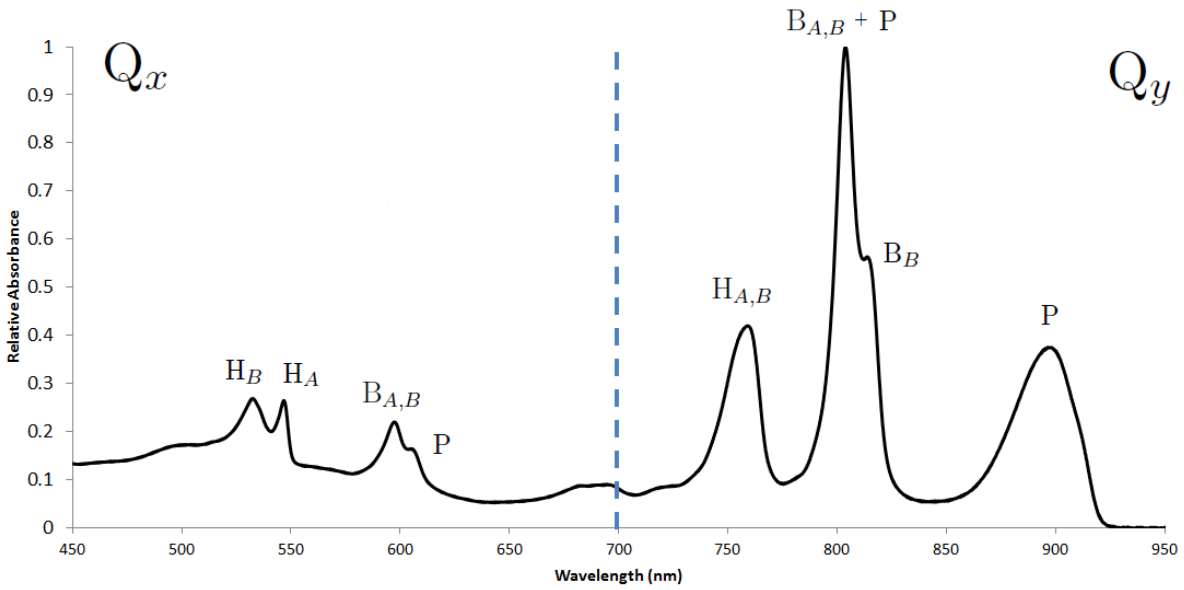

Figure 1.6: Low-temperature (~11 K) steady state absorption spectrum of wild type RC. Peaks are labeled with contributing cofactor names. The dashed line divides the spectrum into two regions, Q_x and Q_y, which arise from transitions along the two axes of the cofactor macrocycle. Data provided by R. Saer.

Although the relative peak positions remain the same, the precise wavelength of the peak depends on the transition energy and therefore can change significantly depending on the temperature at which the spectrum is recorded. Hence, in Figure 1.6, the special pair Q_y peak is centered around 895 nm, but is sometimes referred to in the literature as P865 (e.g. [52]) because of its wavelength at room temperature. Other factors that may cause a change in free energy include a change in the central ion, a change in ion coordination, or alteration in the protein environment of the cofactor. The associated change in energy may result in red or blue shifts of a given cofactor's Q_x and/or Q_y peaks, as well as a change in relative breadth and height [73]. For example, a heterodimeric special pair comprising a BPhe and a BChl can be produced by mutating (M)H200 to leucine [42]. The resulting absorption spectrum has a severely diminished, almost absent special pair Q_y transition peak, and a decreased peak height at the special pair Q_x transition peak, as now only one BChl is contributing to these particular transitions (Figure 1,

[42]). The special pair BPhe appears to instead contribute to the $H_{A,B}$ transition peaks, which exhibit slight increases in height over the corresponding wild type peaks.

1.4 Reaction center variants

The *R. sphaeroides* reaction center is remarkably resilient to changes in its primary sequence, maintaining its gross structure even in the presence of multiple point mutations. Several studies have investigated the effect of site-directed mutagenesis of residues situated close to the electronically active cofactors on the positioning and environment of these cofactors, as well as subsequent effects on electron transfer [12, 23, 29, 66, 71, 73]. For instance, McAuley *et al.* found that the substitution of a tryptophan for a tyrosine at position (L)210, close to B_A, caused a decrease in electron transfer [47]. The crystal structure of this variant was solved and it was determined that there had been a shift in the angle of the B_A BChl (Figure 1.7). Although the tilt was small (fewer than 3°), it was nonetheless clearly visible in the electron density maps, highlighting the potential of structural investigation to detect small but impactful changes in cofactor orientation with associated effects on electron transfer.

A great deal of work has also been done on investigating the reasons for the apparent inactivity of the B branch cofactors. A variant RC which performs electron transfer along the B branch has been created, requiring several point mutations in the L and M subunits and an adjustment of the cofactor composition in the A branch [70]. From these and other experiments [54, 76], it can be concluded that the configuration of the protein scaffold surrounding the reaction center cofactors plays a critical role in fine-tuning the free energy gaps between adjacent cofactors in the electron transfer pathway; these gaps in turn determine the direction of electron flow, as well as maintain the high efficiency of energy conversion characteristic of the RC.

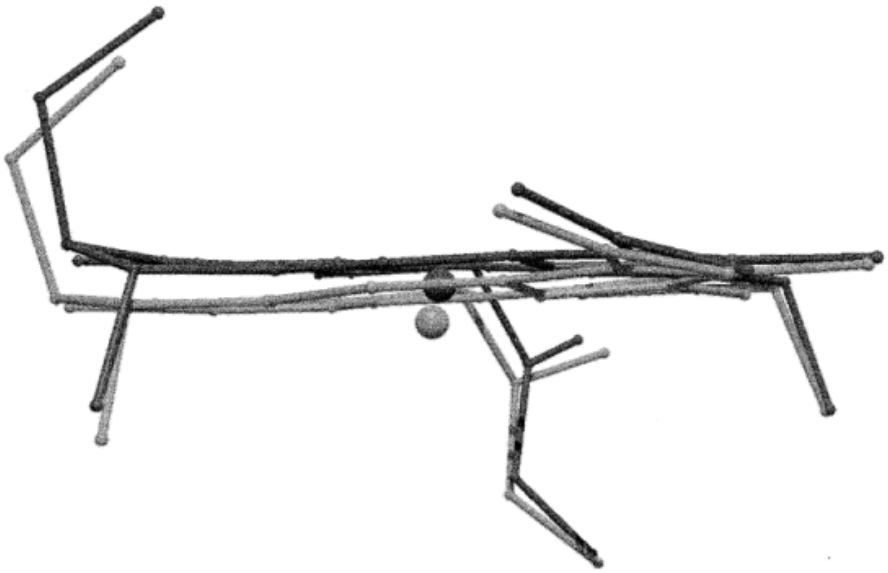

Figure 1.7: Movement of the B_A BChl macrocycle resulting from mutation of the tyrosine at (M)210 to a tryptophan. The cofactor in the mutant RC (light grey) is tilted from that of the WT (dark grey) by approximately 3°.

There have been several studies on means by which cofactor composition can be altered. Each chlorin cofactor in the RC has a residue axial to the plane of the macrocycle [11, 15, 27, 35]. In the wild type RC, this residue is always histidine when the cofactor is BChl, the imidazole group of which acts as a fifth ligand for the Mg^{2+} ion. For BPhe, the adjacent residue is a leucine. Mutating the histidines to a residue unable to ligate the magnesium, including phenylalanine as well as leucine, can result in the substitution of a BPhe for the BChl [12]. Conversely, mutating the leucine to a liganding residue results in the substitution of a BChl for a BPhe. One example of this is of particular interest to the present study: (M)L214H, the β mutant.

1.4.1 (M)L214H, the β mutant

In 1991 Christine Kirmaier *et al.* [41] found that replacing the M subunit L214 residue with a histidine resulted in an altered absorption spectrum for the RC, notably the appearance of a Q_y peak at 785 nm and a Q_x peak increase at 600 nm, accompanied by

a decrease at 760 and 545 nm, the regions indicative of BPhe presence. Based on this and other evidence, later supported by a crystal structure of the variant reaction center [15], Kirmaier concluded that the accessory H_A BPhe had been replaced by a BChl. This was denoted as a β BChl, giving rise to the common description of (M)L214H as "the β mutant". After measuring electron transfer kinetics, it was found that although charge separation still occurred, the quantum yield of the reaction was only 60 % of wild type efficiency. The authors hypothesized that the decrease in the free energy gap between B_A and H_A led to an increased rate of charge recombination ($P^+B_A^- \rightarrow P$) relative to that of electron transfer to the quinone ($P^+B_A^- \rightarrow P^+Q_A^-$). The mechanism by which a BChl is incorporated into H_A rather than a BPhe was not determined.

1.4.2 The Zn-RC

Another notable variant reaction center was discovered in 2007 by Jaschke and Beatty [32]. The authors found that a *R. sphaeroides* mutant lacking the magnesium chelatase gene ($\Delta bchD$) had neither BChl nor BPhe cofactors present in the cell. In their place, the RC assembled with a cofactor structurally similar to BChl, but with a central Zn^{2+} ion instead of Mg^{2+}, henceforth referred to as "Zn-BChl". These Zn-BChls occupy the 6 spaces formerly occupied by BChl and BPhe cofactors in this RC, henceforth referred to as the Zn-RC. Surprisingly, although these cofactors are "unnatural" and moreover, the $H_{A,B}$ cofactors are identical to those in the $B_{A,B}$ site, Lin *et al.* [45] found that the rate of electron transfer from P^* to $P^+H_A^-$ was comparable to that of the WT RC. It was suggested that this is possible because despite the change in absolute free energy values, the potential difference of the P^* to $P^+H_A^-$ reaction is sufficiently similar to maintain the same rate of forward electron transfer. Specifically, it was posited that Zn-BChls at the $H_{A,B}$ sites were tetracoordinated rather than pentacoordinated as in the P and B sites, and therefore more similar in reduction potential to the naturally occurring BPhe than to BChl.

An analogue of the β mutant was made by mutating L214 to histidine in the $\Delta bchD$ background, with the goal of providing a fifth ligand for the H_A Zn^{2+}, causing it to be pentacoordinated. This will be referred to as the Zn-β-RC. When both RCs are referred to, the term "Zn-BChl-containing-RCs" will be used. Spectroscopic investigation of the Zn-β-RC [51] found that the 560 nm band representing the Q_x transition for tetra-coordinated H site Zn-Bchls was absent. This was unexpected, as one would expect that even if the H_A Zn^{2+} was pentacoordinated, the H_B Zn^{2+} would remain tetra-coordinated and therefore give rise to a small 560 nm Q_x peak. The authors suggested several possible explanations, including: a) the H_B cofactor is in fact absent from both the Zn and Zn-β-RCs, and so the 560 nm band represents the electronic contribution of H_A only; b) both Zn-BChls in H sites are pentacoordinated in the Zn-β-RC and tetra-coordinated in the Zn-RC.

1.5 Objective of the present study

1. Substitutions at residue (M)L214. To expand on previous work investigating the effects of substitutions at residue (M)L214, a series of mutants at this site was made and their structures determined by X-ray crystallography. These mutants fell into two categories: aliphatic non-polar residues (glycine and alanine) and amide residues (asparagine). The former category was used to investigate whether the size of the residue had an effect on the dechelation of the central magnesium ion to produce a BPhe at the H_A site, as well as any other structural impacts. The latter was to investigate whether an amide oxygen could ligate the magnesium in the same manner as the histidine nitrogen and if this was sufficient to result in the presence of a BChl in the H_A pocket.

2. Zn-RC and Zn-β-RC. Heretofore, there have been no structures of Zn-BChl-containing RCs. To determine any structural impacts from the substitution of the natural chlorins with Zn-BChls, crystallization experiments were undertaken with the goal of

solving the structures of these two proteins. Additionally, structural investigation could a) confirm the coordination of the H_A Zn-BChl Mg^{2+} and b) suggest an explanation for the absence of the $H_{A,B}$ 560 nm Q_x band in the Zn-β RC.

Chapter 2

Materials and Methods

2.1 RC purification

Reaction centers were purified using a modified version of the protocol of Goldsmith and Boxer [26]. The cells from 21 L of the *R. sphaeroides* semiaerobic culture were collected by centrifugation, and the cell paste was resuspended in 10 mM Tris-HCl (pH 8.0), 150 mM NaCl,and 2 mM MgCl to a volume of 175 mL. A few crystals of DNase I were added to the suspension before the cells were lysed in a French press at 18,000 psi. Lysed cells were centrifuged to pellet debris and unbroken cells. The supernatant was then centrifuged at 66,300 g and 4°C overnight to pellet chromatophores. Following ultracentrifugation, the supernatant was discarded and the remaining pellet was resuspended in 10 mM Tris (pH 8.0) and 150 mM NaCl to a volume of 100 mL. Samples (1 mL) of this suspension were placed in 1.7 mL microcentrifuge tubes and brought to room temperature, and lauryldimethylamine oxide (LDAO, Fluka) was added to each tube at concentrations ranging from 0.5 to 2.75 % to determine the optimal concentration of detergent for RC solubilization. These samples were rocked in the dark for 30 min, and 900 μL was centrifuged at 107,400 g for 30 minutes at 4°C. The 875 nm absorbance maximum of the supernatants was used as a measure of the degree of photosynthetic complex solubilization. In these experiments, the optimal concentration of LDAO for chromatophore solubilization varied between 1.25 and 1.75 %.

Once the optimal LDAO concentration was found, the remaining chromatophore suspension was brought to this detergent concentration and stirred in the dark for 30 min at room temperature, and centrifuged at 117,700 g and 4°C for 15 minutes. The super-

natant solution was collected, and imidazole (10 mM) and NaCl (200 mM) were added to the indicated concentrations before the mixture was loaded onto a Ni-NTA column (Qiagen). The column was washed with 10 mM Tris (pH 8.0), 150 mM NaCl, and 0.1 % LDAO until the maximal absorbance over the range of 500-950 nm was less than 0.01. The RC was eluted from this column with 10 mM Tris (pH 8.0), 150 mM NaCl, 300 mM imidazole, and 0.1 % LDAO, then dialyzed against 10 mM Tris (pH 8.0) and 0.1 % LDAO (TL buffer). His-tagged Zn-BChl-containing RCs were isolated in a similar fashion, except that Zn-BChl-containing RCs were dialyzed against 10 mM Tris, 0.025 % LDAO (Zn-RC-TL buffer). To obtain sufficient amounts of Zn-BChl-containing RCs, the cell culture volume was scaled up to 72 L because of the low yield of these RCs from $\Delta bchD$ mutant strains.

For crystallization, RCs were purified further by anion exchange chromatography with an AKTA Explorer FPLC system (GE Healthcare) equipped with a SourceQ column and elution with a NaCl gradient (0 to 200 mM), with the majority of RCs eluting at 120 mM NaCl. The eluted RCs were desalted by being passed through a 10DG column (Bio-Rad) and concentrated with an Amicon 30 kDa centrifugal ultrafilter (Millipore). RCs used for crystallization experiments were never frozen and crystallization drops were set up immediately following purification.

2.2 Spectroscopy

Low-temperature absorption spectroscopy. Cryogenic absorption spectra (0.6 nm bandwidth) were obtained at ~10–13 K using a Cary 6000 spectrophotometer (Agilent) equipped with a closed-cycle helium cryostat (Omniplex OM-8, ARS Inc.) as described by Lin *et al.*[45]. RC samples and Zn-BChl-containing-RC samples, in TL buffer and Zn-RC-TL buffer respectively, were concentrated to an A_{802} of ~40 by centrifugation using a 30 kDa cutoff Centricon ultrafilter (Millipore). Samples were supplemented with sodium

ascorbate (final concentration of 1 mM) and diluted 1:1 with spectroscopic grade glycerol prior to being frozen between two quartz plates separated by an ~25 μm polycarbonate spacer. Where necessary, a monotonic increase in background absorbance (500 to 730 nm) resulting from light scattering was corrected by subtracting a linear function.

2.3 X-ray crystallography

Fresh solutions of the RC, purified as described in Section 2.1, were used to set up hanging drop crystallization trials. Instead of mixing a reservoir solution with the protein, a separate precipitant solution of 1 M potassium phosphate (pH 7.4), 3.5 % 1,2,3-heptanetriol, and 0.1 % LDAO was prepared and mixed with the protein solution on cover slips before sealing over the reservoir. Various ratios of precipitant and protein solution were found to result in crystals of widely varying quality. Diffraction quality crystals of (M)L214G (~0.3 mm × 0.3 mm × 0.3 mm) grew at a ratio of 2 μL of RC solution (7 mg/mL, or 20.6 OD_{802}/mL) to 1 μL of precipitant solution at 298 K, protected from light, over a reservoir of 1.52 M potassium phosphate buffer (pH 7.4). Crystals appeared after approximately 72 h. Repeated exposure of the crystals to light appeared to diminish diffraction quality, so immediately after the initial exposure to light, crystals were transferred to a solution of 1 M potassium phosphate buffer (pH 7.4) and 30 % glycerol before being flash-frozen in liquid nitrogen. All other crystals used in this work were produced and frozen in a similar fashion, with a concentration of protein solution between 3-9 mg/mL, protein:precipitant ratios between 1:1 to 3:1, and potassium phosphate buffer (pH 7.4) from 1.5-1.6 M.

2.4 Data collection, processing, and structure solution

(M)L214 RC Mutants. Diffraction data from a single (M)L214G crystal were collected at the Canadian Light Source on beamline ID-1 and processed using AUTOXDS, Pointless, and Scala to 2.2 Å resolution [38, 75]. Data sets for (M)L214A and (M)L214N crystals were collected at the Stanford Synchrotron Radiation Lightsource on beamline 7-1 and processed using HKL2000 [53] for (M)L214A, or using Mosflm, Pointless, and Scala for (M)L214N [43, 75]. All three mutant RCs crystallized in space group $P3_12_1$, with one molecule in the asymmetric unit. The solvent content was approximately 75 %, which is typical for a membrane protein crystal. All data sets were isomorphous with the wild-type RC (PDB entry 2J8C, which was chosen as the starting model because it is the highest-resolution (1.85 Å) RC structure in the PDB). The (M)214 mutant structures initially underwent five cycles of rigid body refinement with Refmac5 [50]; the input model used was an edited version of PDB entry 2J8C, with residue (M)L214 changed to the appropriate side chain. Subsequently, models were improved first by alternating between inspection of $2F_o$–F_c and F_o–F_c electron density maps and manual editing in Coot [19], and followed by restrained refinement with Refmac5. Manual editing consisted primarily of adding and removing solvent molecules (primarily water, but also glycerol, 1,2,3-heptanetriol, and LDAO). Water molecules were added using >3 σ peaks in the F_o–F_c difference map with plausible hydrogen bonding geometry. The restrained refinement used a geometry weighting term of 0.25, and the standard CCP4 library files were used for refinement of all cofactors [69]. To generate omit difference density maps, the occupancies of the phytyl tail atoms from CGA to C20, as well as LDAO and/or glycerol, were set to 0, and the model was refined by eight cycles of restrained refinement in Refmac5. Unweighted omit maps were generated using the FFT program in the CCP4 suite [75]. Data collection and refinement statistics are listed in Table 3.1.

Zn-BChl-containing-RCs. Diffraction data were collected at Stanford Synchrotron Light Source on beamline 7.1 using a wavelength of 1.127 09 Å and processed with Mosflm and Aimless to 2.85 Å resolution [43, 75]. Anomalous differences were detected to 6 Å resolution. As with the (M)L214 RCs, all data sets were isomorphous with wild type RC, which was used as the starting point for refinement with removal of the Mg^{2+} ions and, for the Zn-β-RC, the side chain atoms of (M)214. Initial phases were obtained by limited refinement with Refmac5 and F_o–F_c and anomalous difference maps were computed with Coot and FFT, respectively. Based on the peaks observed in both maps, Zn-BChl was modeled at each of the P, B, and H cofactor sites in both the A and B branches. Density for a histidine side chain was observed at residue (M)214 in the Zn-β-RC and modeled accordingly using Coot. Refinement of the structures was continued with Refmac5 and the removal of solvent atoms with unrealistic B-factors.

Chapter 3

Results

3.1 Structural changes in variant RCs with a substitution in (M)L214

3.1.1 Low-temperature spectroscopy

Low-temperature (~11 K) spectroscopy was performed on the (M)L214G and (M)L214A mutants and their spectra were compared with each other as well as with the wild-type RC. Several notable differences were observed, as shown in Figure 3.1. Most obvious are the changes in the Q_x H_A transition peak near 545 nm (dashed line in Figure 3.1B); in both (M)L214G and (M)L214A, this peak exhibits a blue shift such that it merges partially with the 535 nm H_B Q_x transition. The Q_y H_A transition peak (first dashed line in Figure 3.1A) similarly exhibits a blue shift in the two variants, although this effect is much more pronounced in (M)L214G. Regarding transitions associated with BChl rather than BPhe, the special pair Q_x peak is minimally affected, while the Q_y peak (third dashed line in Figure 3.1A) evinces a slight blue shift, again to a greater extent in (M)L214G than in (M)L214A. A greater change is seen in the accessory BChl Q_y transition (second dashed line in Figure 3.1A): the long-wavelength side shoulder, which is thought to be associated with the inactive B_B BChl, appears to have increased in amplitude in both variants, and the primary peak to have decreased substantially in amplitude in (M)L214G.

The 11 K absorption spectra of the RC variants containing a polar residue at (M)214 differ significantly from the spectrum of the wild-type protein, resembling that of the

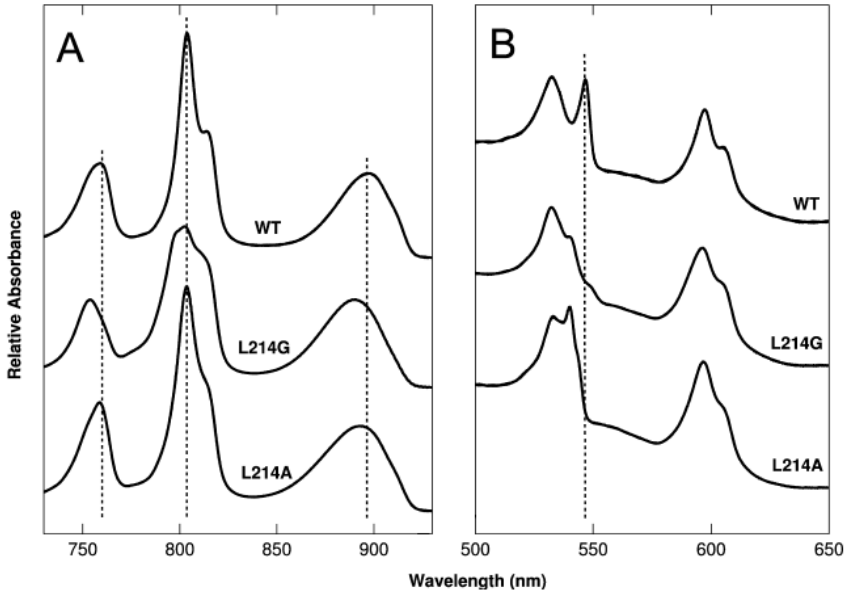

Figure 3.1: Low-temperature (~11 K) steady state absorption spectra of the (A) Q_y and (B) Q_x transitions of the nonpolar (M)214 mutant series. Spectra were normalized with respect to the Q_y absorption maximum of the dimer (P) BChl peaks at 895 nm. The dashed lines mark the Q_x and Q_y absorption peak wavelengths of H_A, as well as the peak wavelengths for the Q_y transition of P and B_A/B_B, in the spectrum of the wild-type RC. Taken from [60].

"β-type" RC variant (M)L214H in important ways (Figure 3.2). For example, in the spectrum of the (M)L214N mutant, a new absorbance band was observed at 785 nm (denoted β), and the absorbance that remained at 756 nm is decreased relative to the amplitude of the P BChl absorbance band. In other words, it appears that the absorbance intensity associated with the Q_y transition of a BPhe group has been replaced with the corresponding absorbance of a new BChl group. In addition, there is an increase in the intensity of the B_A BChl absorbance band of the (M)L214H and (M)L214N mutants, where the β and B_A absorbance bands overlap.

The Q_x transition spectra of the (M)L214N and (M)L214Q mutants confirm the conclusion that these RCs are β-type (Figure 3.2B). As in the (M)L214H control, the peak around 540 nm is absent from the absorbance spectra of the (M)L214N and (M)L214Q

mutants, indicative of a loss of the H_A BPhe from these RCs. There is a corresponding increase in the (M)L214H/Q RC absorbance around 595 nm, indicating the presence of BChl that was absent from the wild-type RC. In the (M)L214H mutant, the BChl Q_x region has an increased amplitude at ~595 nm while retaining the ~605 nm shoulder. This Q_x absorbance profile is thought to be representative of the additional BChl, and the corresponding loss of BPhe, at H_A [29, 41]. However, in the amide-containing (M)L214N and -Q RCs, this ~595 nm peak is blue-shifted relative to those of the wild-type and (M)L214H mutant RCs. The shift is roughly 5 nm in (M)L214N and ~1-2 nm in (M)L214Q.

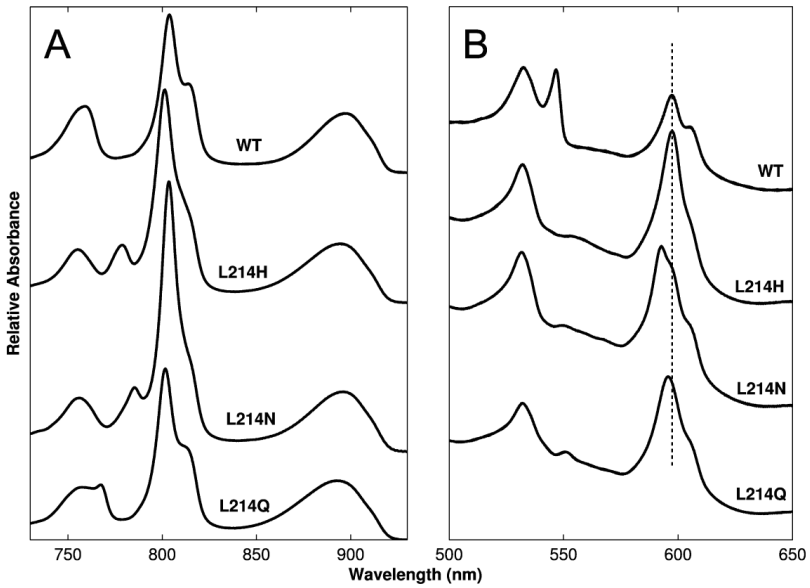

Figure 3.2: Low-temperature (~11 K) steady state absorption spectra of the (A) Q_y and (B) Q_x transitions of the (M)L214N and (M)L214H mutants. Spectra were normalized with respect to the Q_y absorption maximum of the dimer (P) BChl peaks at ~895 nm. The dashed line indicates the absorption peak wavelength of the BChl Q_x transition in the spectrum of the wild-type RC. Taken from [60].

3.1.2 X-ray crystal structures

To identify structural changes in the RC that might account for these spectroscopic shifts, such as changes in the positions of H_A and B_A, the crystal structures of these

three mutant RCs were determined to resolutions of 2.20 to 2.85 Å (Table 3.1). The protein backbones of all three mutant RCs were almost identical to that of the wild-type protein (PDB entry 2J8C, r.m.s.d. of <0.15 Å for all CA atoms). The overall quality is reasonable, with all three structures at the 50th percentile or better in PDB metrics (R_{free}, clash score, Ramachandran outliers, sidechain outliers, and real-space R-value Z-score [RSRZ]) when compared to other structures of similar resolution [8]. There are 3–4 Ramachandran outliers in each structure, three of which are found consistently in other RC structures. The data completeness is high and coordinate error is below 0.2 Å (Table 3.1).

Table 3.1: X-Ray Data Collection and Refinement Statistics for (M)L214G, (M)L214A, and (M)L214N RCs.

	(M)L214G	(M)L214A	(M)L214N
PDB Entry	4IN5	4IN6	4IN7
unit cell parameters (Å)			
$a = b$	139.11	139.03	139.14
c	184.69	184.34	185.14
resolution (Å)[a]	60.24-2.20	60.00-2.70	38.54-2.85
	(2.32-2.20)	(2.75-2.70)	(3.00-2.85)
unique reflections	105008	56265	48933
R^a_{merge}	0.085(0.590)	0.154(0.545)	0.098(0.498)
$I/\sigma I^a$	11.3(2.8)	25.7(3.3)	17.2(4.3)
multiplicity[a]	5.5(5.4)	5.9(3.9)	7.2(7.3)
completeness[a](%)	99.9(100.0)	98.5(97.8)	99.9(99.9)
R_{work}	0.191	0.189	0.179
R_{free}	0.212	0.225	0.207
Wilson B factor (Å^2)	38.8	53.2	60.9
overall B factor (Å^2)	40.8	41.2	42.5
coordinate error[b] (Å)	0.08	0.16	0.16
rmsd for bond lengths (Å)	0.018	0.019	0.020
rmsd for bond angles (°)	1.91	2.18	2.27

[a]Numbers in parentheses reflect statistics for the highest-resolution shell. [b]Coordinate error is the estimated standard uncertainty from maximum likelihood refinement.

In the crystal structures of the (M)L214G and (M)L214A mutant RCs, no difference from the wild-type RC in the location of the H_A BPhe was observed within coordinate error. The H_A chlorin was well-defined but lacked the electron density that would indicate

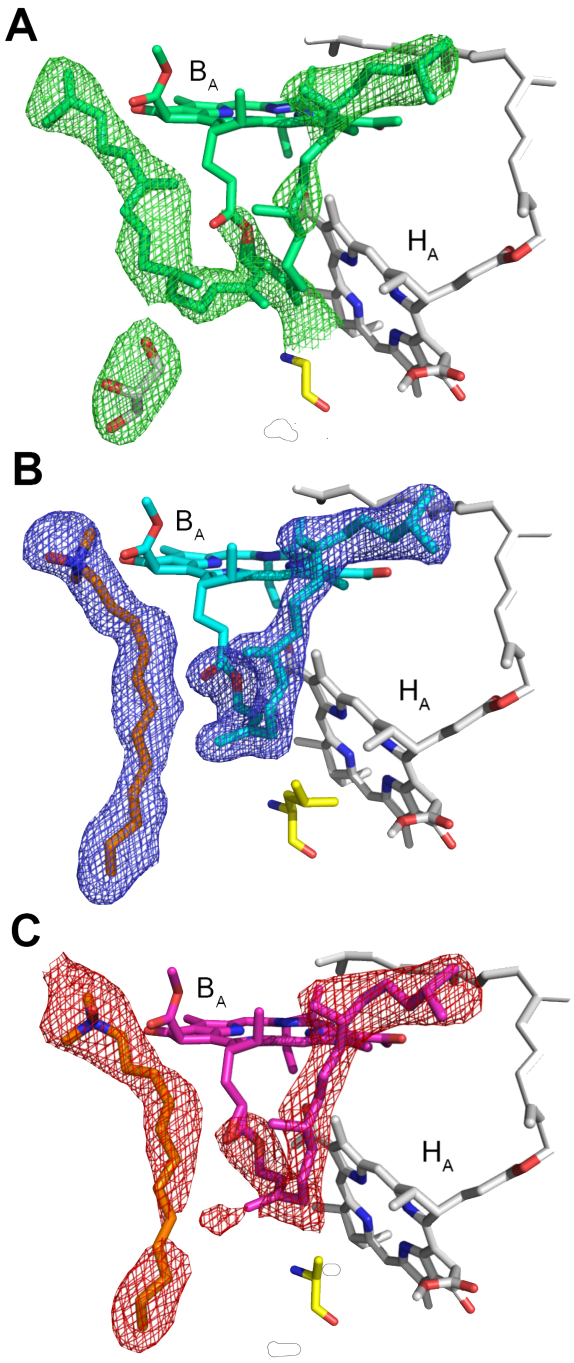

Figure 3.3: Omit difference electron density maps of (A) the (M)L214G RC, (B) the wild-type RC (PDB entry 2J8C), and (C) the (M)L214A RC. These maps were generated by setting the occupancy of the phytyl tail and the nearby LDAO (if present) to zero, followed by eight cycles of refinement. Discontinuous density is visible in the right conformation of the (M)L214G variant, and continuous density for the left conformation can also be seen. Electron density meshes are contoured at 3.0 σ and carved in a 2.5 Å radius. Oxygen atoms are coloured red and nitrogen atoms blue. Carbon atoms are coloured orange for LDAO, gray for glycerol and H_A, yellow for residue (M)214, and green, cyan, and magenta for the (M)L214G, wild-type, and (M)L214A RCs, respectively.

a metal chelated in the macrocycle, consistent with the interpretation that the H_A pocket contains a BPhe. However, there were clear differences in electron density in the vicinity of (M)214 in addition to the mutations themselves. These differences were clearest in the highest-resolution structure of the (M)L214G mutant RC. In this structure, electron density around the phytyl tail of B_A was discontinuous in the region where the tail bends, near the C4 methyl group (Figure 3.3A), implying that the B_A tail is disordered. Notably, the bend in the phytyl tail is discernible and in the proximity of residue (M)L214 in the wild-type RC (Figure 3.3B).

The volume made available by the deletion of the leucine side chain in the (M)L214G mutant RC is occupied in part by the rotation around the phytyl tail bend. By inspection of difference omit maps, the B_A phytyl tail was modeled in two conformations with equal occupancy. The "right" conformer depicted in Figure 3.3A is equivalent to the conformation observed in the wild-type *R. sphaeroides* RC (Figure 3.3B). In the "left" conformation, also shown in Figure 3.3A, the B_A phytyl tail is directed away from the H_A macrocycle such that a portion of H_A is exposed to the solvent. In this conformer, the phytyl chain and a glycerol (cryoprotectant) molecule displace the LDAO molecule that occupies this space in the structure of the wild-type RC (compare panels A and B of Figure 3.3).

The two conformers and glycerol molecule do not completely account for the difference density present in sigma-weighted and unweighted maps at the mutation site or in the region of the two phytyl tail conformations, suggesting that partially occupied solvent molecules and perhaps additional conformations of the phytyl tail are present. The difference maps derived from the (M)L214A crystal diffraction data are consistent with the two conformations of the phytyl tail (Figure 3.3C), although the lower quality of the (M)L214A data restricts structural comparisons with the (M)L214G structure to the mutation site.

In the (M)L214N crystal structure, positive difference electron density was obvious at the center of the chlorin macrocycle in the H_A position (Figure 3.4). This density was modelled as a Mg^{2+} ion, confirming that the chlorin at this position is a BChl group. After subsequent refinement, the B factor associated with the Mg^{2+} ion was commensurate with the BChl ring, and no residual difference density was present. At residue (M)214, adjacent to the Mg^{2+}, density for an asparagine side chain was present and modeled accordingly. The (M)N214 OD2 atom is located approximately 2.0 Å from the Mg^{2+}; the Mg^{2+} to OD2 bond angle is approximately perpendicular to the plane of the macrocycle, and the Mg^{2+} ion is displaced ~0.4 Å from the plane formed by the tetrapyrrole N atoms toward the new ligand, supporting the assignment of a metal–ligand bond. A similar 0.4 Å displacement of Mg^{2+} from the plane was observed in the equivalent N–Mg^{2+} bond between (L)H153 and the B_A BChl. The ND1 atom of (M)N214 is within H-bond distance (3.1 Å) of the main chain carbonyl of (M)Y210. The alternative amide conformation of the asparagine side chain with Mg^{2+} coordination by the ND1 atom of Asn214 is unlikely because of the inability of the OD2 atom to establish a hydrogen bond with this main chain carbonyl group, and because of the requirement for the metal to displace a proton of the NH_2 group to form a metal—N ligand. Furthermore, the lone electron pair of the amide nitrogen atom should participate in a resonance structure of the amide group, resulting in a partial positive charge on the nitrogen.

3.2 Structural characterization of Zn-BChl-containing-RCs

X-ray crystallography and anomalous scattering. To elucidate the type, coordination state and occupancy of the bacteriochlorin cofactors in Zn-BChl-containing RCs, the crystal structures of the Zn-RC and Zn-β-RC were solved to a resolution of 2.85 Å. Completeness is somewhat lower for these structures than for the series of (M)L214

Table 3.2: X-Ray Data Collection and Refinement Statistics for the Zn and Zn-β RCs.

	Zn-RC	Zn-β-RC
PDB Entry	4N7K	4N7L
unit cell parameters (Å)		
$a = b$	139.45	139.59
c	184.18	184.05
resolution (Å)[a]	73.23-2.85	69.79-2.85
	(2.90-2.85)	(2.90-2.85)
unique reflections	46994	42741
R^a_{merge}	0.105(0.972)	0.098(0.705)
$I/\sigma I^a$	10.5(1.5)	12.6(2.4)
multiplicity[a]	6.2(4.7)	7.0(6.2)
completeness[a](%)	96(95)	87.4(85.6)
R_{work}	0.182	0.167
R_{free}	0.242	0.216
Wilson B factor (Å^2)	53.1	47.0
overall B factor (Å^2)	58.2	54.8
coordinate error[b] (Å)	0.21	0.17
rmsd for bond lengths (Å)	0.011	0.013
rmsd for bond angles (°)	2.6	2.7

[a]Numbers in parentheses reflect statistics for the highest-resolution shell. [b]Coordinate error is the estimated standard uncertainty from maximum likelihood refinement.

mutants, but nonetheless both structures are at the 50th percentile or better in PDB metrics, compared against structures of similar resolution [8]. The Zn-RC and Zn-β-RC structures had 7 (0.8 %) and 6 (0.7 %) Ramachandran outliers respectively, slightly more than in the (M)L214 series structures. The refinement statistics can be seen in Table 3.2. Overall, the structures resemble that of the native RC (PDB entry 2J8C). In both the Zn-RC and Zn-β-RC structures, the iron, carotenoid and all the bacteriochlorin cofactors are present. An electron density map was computed from the anomalous difference data collected above the Zn-edge of the two RC structures to reveal the location of Zn^{2+} ions within the two structures (Table 3.3). A peak greater than 4 σ was observed in the anomalous maps at the center of all bacteriochlorin-type cofactors, indicative of the presence of Zn^{2+} ions at these sites. At the wavelength used for data collection, the anomalous signal from Mg^{2+} is weak and would not significantly contribute to the den-

sity observed in the map. The signal from iron can be used as an internal standard, and indeed, peaks at 8.7 σ and 10 σ were observed at the iron site in the Zn-RC and Zn-β-RC structures, respectively. In the Zn-RC structure, five of the bacteriochlorin cofactors appear to be bound at full occupancy based on refined Zn^{2+} ion B-factors of (58 $Å^2$) or less and anomalous map peaks >12 σ. In contrast, the larger B-factor of the Zn atom at H_B site (86 $Å^2$), in combination with the anomalous map peak (7σ), implies a lower occupancy and/or a higher degree of disorder of this cofactor. The H_B cofactor in the Zn-β-RC structure exhibits even lower occupancy and/or greater disorder (Table 3.3).

Table 3.3: Anomalous map statistics for metals in the Zn-RC and Zn-β-RC X-ray diffraction datasets.

Site	Zn-RC				Zn-β-RC			
	Omit Fo-Fc peak (σ)	Anom. map peak (σ)	Zn B-factor ($Å^2$)	Leu/His-Zn distance (Å)	Omit Fo-Fc peak (σ)	Anom. map peak (σ)	Zn B-factor ($Å^2$)	Leu/His-Zn distance (Å)
P_A	25	13	50	2.1	25	16	43	2.2
P_B	25	13	50	2.1	24	14	44	2.2
B_A	25	14	44	2.4	25	15	39	2.3
B_B	24	14	39	2.4	25	16	37	2.5
H_A	20	12	58	3.2	26	15	43	2.3
H_B	13	7	86	3.6	11	4	113	3.9
Fe	24	9	45	–	24	10	41	–

These values for the H_B cofactor in both the Zn-RC and Zn-β-RC, relative to the values for the other bacteriochlorin cofactors, indicate that the H_B pocket is not well-occupied, and perhaps less well-occupied in the Zn-β-RC than in the Zn-RC. Interestingly, the B-factors of the amino acid residues surrounding the H_B cofactor were similar to those in the rest of the protein, indicating that the observed disorder was centered on the Zn-BChl molecule itself, and not the surrounding protein. In comparison to the H_B site, the B_B, $P_{A/B}$, and A-branch Zn-BChls of the Zn-β-RC and Zn-RC appear to be relatively well-ordered and fully occupied, based on the anomalous signal intensity and B-factor values, which are similar to the mean values of each respective structure (Table

3.3). A side by side comparison of the H_A cofactors for the Zn-RC and Zn-β-RC can be seen in Figure 3.5. For Zn-BChl in sites with a His residue available for coordination, the imidazole ring is observed 2.1 to 2.4 Å from the Zn^{2+} ion. At the Zn-RC H_A site (with a leucine present), the side chain is separated by 3.2 Å from the Zn^{2+} ion of the Zn-BChl. Although at 2.85 Å resolution for these structures the error estimate of these distances is ± 0.3 Å, the electron density maps indicate the absence of an externally-derived metal ligand, such as water, at all of the Zn-BChls. Therefore, it appears that the major structural difference between the A-branch electron transfer carriers in the Zn-RC and Zn-β-RC is the coordination state of the Zn^{2+} ion in the H_A Zn-BChl, which is 4-coordinate in the Zn-RC and 5-coordinate in the Zn-β-RC.

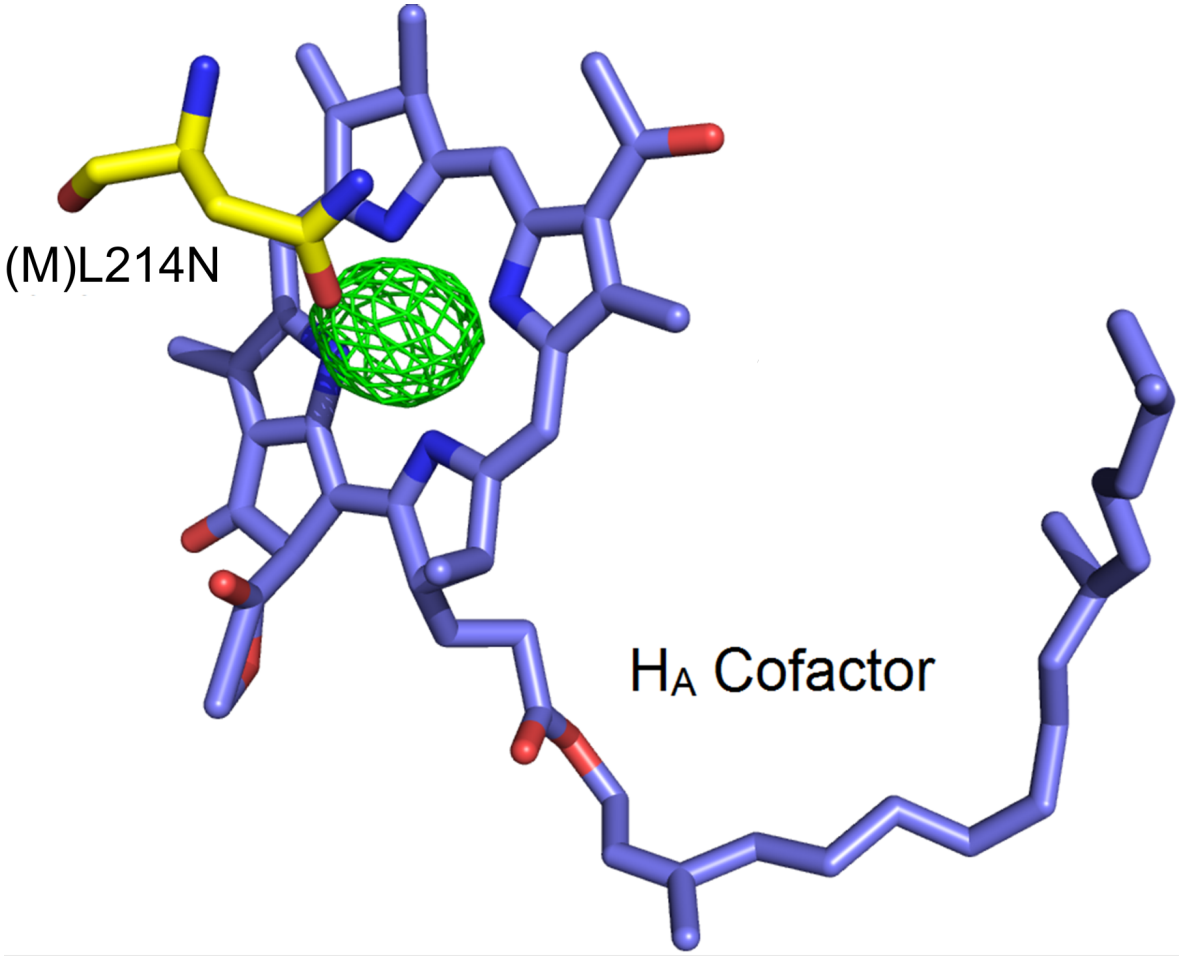

Figure 3.4: Omit difference electron density map of the (M)L214N RC, illustrating positive difference density for the Mg^{2+} ion at the center of the chlorin ring of BChl in the H_A site. The electron density mesh is contoured at 4.0 σ and carved in a 2.0 Å radius. Oxygen atoms are coloured red and nitrogen atoms are blue. H_A carbon atoms are coloured purple and (M)L214N carbon atoms are yellow.

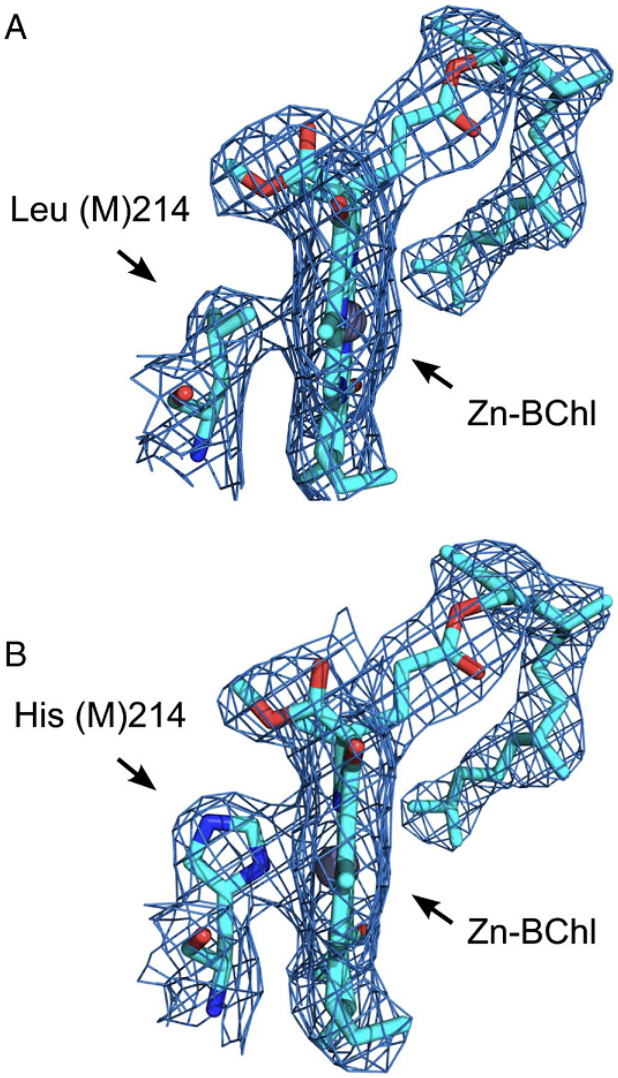

Figure 3.5: Stick models and electron density (mesh) of the H_AA cofactor and axial (M)214 residues from the crystal structures of the (A) Zn-RC and (B) Zn-β-RC. The distances from the axial residues to the macrocycle centers are 3.9 and 2.1 to 2.4 for the Zn-RC and Zn-β-RC, respectively. Colour code: teal, carbon atoms; blue, nitrogen atoms; red, oxygen atoms. Reprinted from [61] with permission.

Chapter 4

Discussion

4.1 Structural changes in variant RCs with a substitution in (M)L214

4.1.1 Aliphatic non-polar residues (G,A)

The above data suggest that the size of the adjacent residue is not the determining factor in the presence of BChl or BPhe in the RC H_A pocket. Although it was plausible that this site could dechelate a BChl Mg^{2+} ion through steric exclusion via the bulky (M)L214 side chain, the crystal structures show that the chlorin composition of the P, B, and H sites of the (M)L214G and (M)L214A RCs is the same as in the wild-type protein, despite the lower side chain volumes. Rather, the data suggest that the type of cofactor found in the H_A pocket is determined solely by the presence or absence of an axial residue capable of Mg^{2+} coordination. These results are complementary to and extend previous studies of "cavity mutants" of the *R. sphaeroides* RC, in which His axial ligands to the P BChls were changed to Gly residues, and proposed to introduce a cavity in the vicinity of the P BChls. Although crystal structures were not presented, Stark spectroscopy studies and pigment analysis demonstrated that those RCs assemble with a native pigment composition. Furthermore, water molecules were proposed to act as a fifth ligand to the P BChls in the cavity mutants, and these waters appeared to be switched to other coordinating small molecules by incubation of the RC in the appropriate solute [27].

The results with mutations at H_A enrich our understanding of the complexity in pigment discrimination within RCs by indicating that not all binding pockets conform to a single set of rules when it comes to populating these cofactor binding sites. Although adventitious ligands such as water may compensate for the loss of an imidazole group in the P BChls, such polar ligands do not appear to be suitable as BChl Mg^{2+} ligands when the (M)214 Leu side chain is absent from the H_A pocket. This difference may stem from the fact that the H_A pocket is embedded more deeply in the membrane bilayer than the P region and hence less likely to incorporate water. Instead, the void is occupied in part by an alternative conformation of the phytyl tail of B_A. An analogous structural plasticity in the P region of the RC was found in "heterodimer" mutations in which one of the P BChls was changed to BPhe by substitution of Leu for a His ligand to a BChl Mg^{2+} [12, 42]. In an (M)L214H background, however, a heterodimer failed to assemble, and the resultant RC incorporated two BChls at P for unknown reasons. Those results demonstrated that even when the coordinating axial (M)H202 residue is substituted with a Leu residue, the P binding pocket is capable of incorporating BChl. Although it is conceivable that an adventitious ligand was incorporated into the binding pocket of the P BChls in the (M)H202/(M)L214H double mutant, those results raise additional questions about the nature of pigment selectivity in RCs as well as in the biogenesis of (B)Phe.

The biological production of a pheophytin (Phe) from a Chl is best understood in senescent plant materials. Shioi and co-workers partially purified a heat-stable "magnesium dechelating substance" that catalyzed the conversion of chlorophyllide to pheophorbide [65]. Although this as yet poorly defined low-molecular weight substance was implicated as functioning during leaf senescence, and therefore Chl degradation, the possibility that such a substance could function during Chl synthesis, to yield Phe for incorporation into RCs, cannot be excluded.

Other work on plant material, in this case the source of Phe in the photosystem II RC [30], points to a pre-Chl origin of Phe in which a branch point in the Chl biosynthetic pathway appeared to yield Phe in etiolated leaves. The authors suggested that the magnesium chelatase enzyme itself was responsible for Mg^{2+} removal. Such a branch point has not been reported in the BChl biosynthesis pathway of purple phototrophic bacteria despite extensive mutagenic analyses [74]. Although it is possible that a dedicated dechelating enzyme exists for the synthesis of RC BPhe, a mutant strain deficient in this activity has not been discovered thus far. Moreover, BPhe is functionally present only in RCs, and free BPhe is not found in nonsenescent photosynthetic organisms. Alternatively, it is possible that the local environment of the BPhe-binding pockets within RCs, in general, results in the loss of Mg^{2+} from BChl unless a coordinating ligand specific for the central metal is present. Because of the tendency for this ion to exist only in the penta- or hexacoordinated state in BChl, it is conceivable that the Mg^{2+} is removed from the macrocycle in the H_A site in part because of the absence of a fifth coordinate.

An interesting consequence of substituting (M)L214 with small-volume, nonpolar side chain residues in the *R. sphaeroides* RC is the shifting of the Q_x transition corresponding to the H_A BPhe to a higher energy. It was previously suggested by Bylina *et al.* that an analogous blue shift may be attributed to changes in the hydrogen bonding interaction between the H_A BPhe macrocycle and a nearby Glu at position (L)104 [11]. Specifically, when (L)E104 was changed to a weaker proton donor (Gln) or to another residue incapable of hydrogen bonding to the BPhe (Leu), the Q_x absorbance maximum of H_A became more similar to that of H_B. In the case of an RC (L)E104L mutant, the Q_x transitions of H_A and H_B were almost overlapping. A similar blue shift was observed in the (M)L214G and (M)L214A mutants (Figure 3.1B), but the crystal structures show that these shifts are independent of changes in macrocycle hydrogen bonding interactions. Potentially, the changes in the Q_x transition of H_A observed in the (M)L214G

and (M)L214A mutants are induced by the disorder in the B_A phytyl tail, and related changes in the binding of detergent and possibly disordered water molecules.

The X-ray structures of the (M)L214G and (M)L214A mutants reveal that this residue affects the orientation of the B_A phytyl tail (Figure 3.3) and offer an explanation for the changes in the low-temperature absorbance spectra of the RCs with these low volume side chains. Although the influence of the phytyl tail in the direct tuning of the electrochemical midpoint potential of a chlorin is not well understood and considered to be negligible, the tail was thought to affect the packing of nearby protein residues and other chlorins [62]. The crystal structures indicate that, other than the substituted side chain itself, there is not a direct effect of the (M)214 side chain substitution on the electronic properties of H_A (*i.e.*, there appear to be no changes in the distance between the H_A macrocycle and protein atoms that would give rise to changes in the electronic properties of the H_A BPhe). Therefore, the absorbance changes in the Q_x and Q_y transitions of H_A appear to stem predominantly from changes in the B_A phytyl tail and perhaps disordered water, as an indirect effect of the substitution of (M)L214 with smaller, nonpolar moieties. These mutational changes are also accompanied by a broadening of the Q_y absorbance band of B_A in the (M)L214G mutant (Figure 3.1), perhaps reflecting a population of mutant RCs that assume a range of alternative B_A phytyl tail configurations, as indicated by the crystal structure.

Although the X-ray diffraction data from (M)L214A RC crystals indicate that some degree of B_A phytyl tail disorder is present (Figure 3.3C), this disorder appears to be less than in the (M)L214G RC crystal, as electron density for the right conformation is continuous whereas electron density for the alternative conformation is weaker. It could be argued that this difference in electron density arises solely from the lower resolution of the (M)L214A data relative to the resolution of the data for the (M)L214G structure, but in the absorbance spectra, the broadening of the BChl B_A Q_y band is seen most

prominently in the (M)L214G mutant (Figure 3.1). To a lesser extent, the BChl B_A Q_y band is also broadened in the (M)L214A RC without a corresponding increase in the amplitude of the band. In combination with the similarities between the (M)L214A and (M)L214G Q_x transitions, these data indicate some disorder or motion in the (M)L214A B_A phytyl tail, although it appears to be insufficient to allow the adoption of alternative conformations to the same degree as in the (M)L214G mutant.

The RC contains the electronically active cofactors within well-insulated tunneling pathways that prevent molecules such as intramembrane quinones from interacting with RC pigments and thus potentially affecting rates of electron transfer. *In vivo*, the RC is surrounded by LH1, which may act as a barrier between the quinone pool and the RC [7, 44, 57]. However, it was shown that 25-30 % of the native quinone pool is retained in an isolated RC/LH1/PufX preparation, evidently because quinones bind to these proteins and may be located within the space between the RC and LH1. In addition to the insulating shield provided by the RC protein matrix, the long, aliphatic phytyl tails esterified to the BChl and BPhe macrocycles may also serve a similar role, at least *in vitro*.

Although it is plausible that these cofactor hydrophobic tails spontaneously adopt alternative configurations, there has been little account of the mechanisms by which these tails assume their native positions, or what factors might govern their three-dimensional configurations.

The *in vivo* function of *R. sphaeroides* RCs containing these structural perturbations testifies to the robustness of this protein in the catalysis of light-driven excitation energy transduction. However, kinetic analysis of electron transfer reactions in purified RCs reveals that the (M)L214G RC is significantly impaired in ET from H_A to Q_A, as is the (M)L214A RC to a lesser extent [54].

4.1.2 Amide residues (N)

The mutant RCs containing Asn and Gln amide side chains at (M)214 incorporated BChl into the H_A pocket. These proteins resemble the (M)L214H (β-type) mutant RC described by Kirmaier *et al.* [41] in terms of the *in vivo* activity indicated by similarly impaired phototrophic growth kinetics under a low light intensity [60]. However, the absorbance band shifts induced by these three β-type mutations were very different from each other (Figure 3.2). Because the Q_y band shifts of the (M)L214N and (M)L214Q RCs differed more from each other than from that of the (M)L214H RC (Figure 3.2), it appears that the absorption spectra of H_A BChls are not greatly affected by whether the Mg^{2+}-ligating atom is an imidazole nitrogen or an amide oxygen. In these cases, the possibility that the amide nitrogen atom acts as a ligand is excluded because of the participation of the nitrogen's lone electron pair in a resonance structure of the amide group, the location of the ND1 atom of (M)N214 within H-bonding distance of the main chain carbonyl of (M)Y210, and the need for loss of a proton of the NH_2 group to form a Mg^{2+}—N ligand bond.

The side chain of the residue replacing the Leu residue in the (M)L214N, (M)L214Q, and (M)L214H RCs differs in length and volume. The Asn side chain is shorter than the Gln side chain, but it offers equivalent atoms to coordinate the Mg^{2+} ion. The (M)L214N and (M)L214Q RC H_A Q_y absorbance bands differed by ~25 nm (Figure 3.2), so the length and/or volume of the Mg^{2+}-coordinating side chain appears to have a major effect on the energy of the H_A Q_y absorbance band, with the longer Gln side chain resulting in a higher-energy H_A band in the Q_y region. Indeed, studies of BChls in a variety of organic solvents demonstrated that the Q_y transition is sensitive to the nature of the axial ligand to the pigment. Specifically, the Q_y transition shifts to a higher energy when the Mg^{2+} ion approaches the plane of the macrocycle because of a stronger metal—macrocycle interaction (this interaction being strongest in an in-plane Mg^{2+}, as

is the case in hexacoordinated BChls), and vice versa [21, 28]. The distance between the H_A Mg^{2+}-coordinating atom in the (M)L214H side chain and the BChl Mg^{2+} may be intermediate between the distances in the (M)L214N and (M)L214Q RCs; if so, this difference would account for the intermediate position of the H_A Q_y absorbance band relative to the H_A Q_y bands of the (M)L214N and (M)L214Q RCs, but the coordinates of the (M)L214H mutant RC are unavailable.

The available data suggest that the distance between the metal-coordinating atom of the RC protein and the Mg^{2+} ion of (B)Chls, and therefore the position of the Mg^{2+} relative to the plane of the (B)Chl macrocycle, is the major determinant of the Q_y band energy in absorbance spectra, rather than the identity of the coordinating atom (*i.e.*, a His nitrogen atom or an oxygen atom from Asn or Gln). Longer distances of coordinating atoms from the Mg^{2+}, as is the case with Asn, result in a Q_y absorbance maximum at a longer wavelength, whereas shorter distances (as with His or Glu) result in correspondingly shorter wavelengths of Q_y absorbance peaks.

Because the Q_y band shifts of the (M)L214N, (M)L214Q, and (M)L214H RCs must reflect differences in β_A excitation energies, these changes should be reflected in changes in ET rates, as in the original (M)L214H mutant RC [41]. Ongoing time-resolved spectroscopy and structural studies of these new RC variants should yield a deeper understanding of connections between protein side chain composition, pigment content, and catalytic activity in this tractable experimental system.

4.2 Structural characterization of Zn-BChl-containing-RCs

As mentioned above, in the Zn-RC, the B-factor for the protein component surrounding the H_B Zn-BChl is comparable to the average of the structure. This is consistent with

the idea that the RC is a relatively rigid protein, and does not rearrange its folding due to changes in cofactor composition or even when a cavity is created by the lack of a cofactor, as was observed in pigment exclusion experiments on the H_B BPhe [35, 71].

With regard to the cofactors, however, the crystal structures show that, relative to the WT-RC, the Zn-BChl in the H_B pocket of the Zn-RC is bound at less than full occupancy or is highly disordered, and perhaps the occupancy is even lower or disorder greater in the Zn-β-RC (Table 3.3). These conclusions are based on weaker density in omit difference maps of the H_B Zn-BChl, the large B-factors associated with the Zn^{2+} in the H_B pocket, and the low anomalous signal intensities for that Zn^{2+} atom (compare the values for H_B to those of the other cofactors in Table 3.3).

Interestingly, the average B-factor of the H_B BPhe from the highest resolution RC structure currently available in the PDB database is greater than all of the other cofactors, perhaps indicating weaker binding to this pocket in the WT RC as well. Additional evidence for relatively weak binding of BPhe in the WT RC H_B pocket comes from experiments involving substitution of BPhe with plant Phe, as well as a variety of other pigments. These experiments demonstrated that substitution is preferential in the H_B over the H_A site, consistent with a weaker binding of BPhe in the H_B pocket [22, 49]. *In vitro*, the binding pockets for $H_{A,B}$ are selective for pheophytins, as incubation of RCs in a molar excess of metal-containing bacteriochlorins (the standard procedure for pigment exchange) resulted in substitution of pigments at the $B_{A,B}$ binding pockets instead of $H_{A,B}$ [35, 63, 67]. The greater hydrophobicity of BPhe over BChl and Zn-BChl, as indicated by the longer retention time for BPhe in reversed-phase HPLC using a C18 column [32], may be part of the reason why binding of metal-containing bacteriochlorins to the $H_{A,B}$ pockets is weak, although it is not clear why the H_B Zn-BChl may be lost more readily or less efficiently inserted into the RC than the H_A Zn-BChl. Alternatively, it is possible that the Zn-RCs contain partially occupied H_B sites due to an insufficient

quantity of available Zn-BChls in the cell. One important consequence of the *bchD* mutation yielding Zn-BChl-producing strains of *R. sphaeroides* is the severely impaired ability to synthesize the pigment [32, 33]. It is presumed that the inability of the organism to grow photoheterotrophically is because of a paucity in the cellular content of light-harvesting and RC complexes.

Unlike the H_B cofactors of the Zn-RC and Zn-β-RC, the H_A cofactors appear less disordered, suggesting there is no issue with the occupancy of the pocket. From a structural perspective, the H_A cofactors appear to assume a similar configuration in the two Zn-BChl-containing RCs (Figure 3.5), with a possible macrocycle displacement of 0.6 Å between the two RCs. Given the modest resolution of the data obtained for these two RCs, a firm conclusion cannot be made on this geometric displacement between the cofactors; however, the small degree of displacement is consistent with the interpretation that the differences in the functional characteristics of the two Zn-BChl-containing RCs stem from changes in H_A cofactor coordination state.

These results suggest that RCs have a degree of functional tolerance for different cofactors, and that the protein component is a key instrument in the design of an efficient charge separation pathway. The Zn-RC studied here is a case in point, as it contains a cofactor arrangement supportive of a faster rate of ground state recombination from the $P^+I_A^-$ state, but is nevertheless capable of attaining a relatively high efficiency of electron transfer [45]. This is likely because the protein scaffold of the Zn-RC has remained unchanged from its WT-RC counterpart, granting this RC the same favourable cofactor geometries and tunnelling pathways available to the WT-RC. From an evolutionary perspective, this could be advantageous to photosynthetic organisms during periods of environmental change, such as a change in the wavelengths of light available, for it would allow for the continued utilization of existing protein machinery when the production of a new type of chlorin would provide a selective advantage. In such a case, the new pigment

could be incorporated into a protein "template" with suitable geometries, which would grant the organism some degree of charge separation capability, enabling photosynthetic growth. Mutations in protein side chains may later provide further energetic optimization, resulting in a high-efficiency RC that assembles with a new pigment. For this to happen, however, the photosynthetic organism must be able to survive for some time with an inefficient RC to allow beneficial mutations to accumulate. Previous results show that LH2-lacking *R. sphaeroides* strains containing RCs with small nonpolar side chains at H_A retain their ability to grow at low photon fluxes, despite the relatively low efficiencies of these RCs compared to the WT-RC, indicating that purple photoheterotrophs are indeed quite capable of surviving with lower efficiency RCs [60].

4.3 Conclusions and future directions

High-resolution structures of the *R. sphaeroides* RC provide insight into the interactions between the protein environment and photosynthetic cofactors, especially in cases where steady-state absorption spectroscopy provides insufficient detail. In this study, although the precise mechanism for dechelation of BChl in *R. sphaeroides* remains elusive, our understanding of the factors that lead to either a BChl or a BPhe occupying H_A site has been broadened. Structures of (M)L214 variants in addition to those described here could provide even more clarification on the role this important residue plays, and perhaps clarify the causes of peak shifts in their spectra. Moreover, the structures that were determined suggest an additional avenue of investigation: the phytyl tails of the chlorins, which have so far received relatively little attention. Further investigation of possible mobility in these tails could be valuable, perhaps by obtaining and characterizing RCs where the chlorins incorporate a different esterifying alcohol, such as geranylgeraniol or farnesol.

Similarly, the structures of Zn-containing RCs not only provided support for previous

hypotheses on the nature of their cofactors, but also illuminated the intriguing fact that the occupancy of the H_B site is surprisingly low, in not only the Zn-RC but also potentially in the WT RC as well. Kinetic studies and structures of variant RCs where electron transfer occurs through the B-branch cofactors could shed some light on the universality (or lack thereof) of this discovery, and its impact on photosynthetic efficiency. These first-ever structures of Zn-containing RCs can also serve as a foundation for deeper study of this unique variant.

Bibliography

[1] Addlesee, H.A. and Hunter, C.N. (1999) Physical mapping and functional assignment of the geranylgeranyl-bacteriochlorophyll reductase gene, bchP, of *Rhodobacter sphaeroides*. *J. Bacteriol.*, **181**(23), 7248–7255.

[2] Addlesee, H.A. and Hunter, C.N. (2002) *Rhodospirillum rubrum* possesses a variant of the bchP gene, encoding geranylgeranyl-bacteriopheophytin reductase. *J. Bacteriol.*, **184**(6), 1578–1586.

[3] Allen, J., Feher, G., Yeates, T., Rees, D., Deisenhofer, J., Michel, H., and Huber, R. (1986) Structural homology of reaction centers from *Rhodopseudomonas sphaeroides* and *Rhodopseudomonas viridis* as determined by X-ray diffraction. *Proc. Natl. Acad. Sci. U.S.A.*, **83**(22), 8589–8593.

[4] Allen, J.P. and Feher, G. (1984) Crystallization of reaction center from *Rhodopseudomonas sphaeroides*: preliminary characterization. *Proc. Natl. Acad. Sci. U.S.A.*, **81**(15), 4795–4799.

[5] Allen, J.P., Feher, G., Yeates, T.O., Komiya, H., and Rees, D.C. (1987) Structure of the reaction center from *Rhodobacter sphaeroides* R-26: the cofactors. *Proc. Natl. Acad. Sci. U.S.A.*, **84**(16), 5730–5734.

[6] Axelrod, H.L., Abresch, E.C., Okamura, M.Y., Yeh, A.P., Rees, D.C., and Feher, G. (2002) X-ray structure determination of the cytochrome c2: reaction center electron transfer complex from *Rhodobacter sphaeroides*. *J. Mol. Biol.*, **319**(2), 501–515.

[7] Bahatyrova, S., Frese, R.N., Siebert, C.A., Olsen, J.D., Van Der Werf, K.O., Van Grondelle, R., Niederman, R.A., Bullough, P.A., Otto, C., and Hunter, C.N.

(2004) The native architecture of a photosynthetic membrane. *Nature*, **430**, 1058–1062.

[8] Berman, H., Westbrook, J., Feng, Z., Gilliland, G., Bhat, T., Weissig, H., Shindyalov, I., and Bourne, P. (2000). The Protein Data Bank. [Online; accessed 4-May-2015].

[9] Bollivar, D.W. (2006) Recent advances in chlorophyll biosynthesis. *Photosynth. Res.*, **89**(3), 1–22. doi:10.1007/s11120-006-9076-6.

[10] Bollivar, D.W., Wang, S., Allen, J.P., and Bauer, C.E. (1994) Molecular genetic analysis of terminal steps in bacteriochlorophyll *a* biosynthesis: characterization of a Rhodobacter capsulatus strain that synthesizes geranylgeraniol-esterified bacteriochlorophyll *a*. *Biochemistry*, **33**(43), 12763–12768.

[11] Bylina, E.J., Kirmaier, C., Mcdowell, L., Holten, D., and Youvan, D.C. (1988) Influence of an amino-acid residue on the optical properties and electron transfer dynamics of a photosynthetic reaction centre complex. *Nature*, **336**, 182–184.

[12] Bylina, E.J. and Youvan, D.C. (1988) Directed mutations affecting spectroscopic and electron transfer properties of the primary donor in the photosynthetic reaction center. *Proc. Natl. Acad. Sci. U.S.A.*, **85**(19), 7226–7230.

[13] Camara-Artigas, A., Brune, D., and Allen, J.P. (2002) Interactions between lipids and bacterial reaction centers determined by protein crystallography. *Proc. Natl. Acad. Sci. U.S.A.*, **99**(17), 11055–11060. doi:10.1073/pnas.162368399.

[14] Chang, C.H., El-Kabbani, O., Tiede, D., Norris, J., and Schiffer, M. (1991) Structure of the membrane-bound protein photosynthetic reaction center from *Rhodobacter sphaeroides*. *Biochemistry*, **30**(22), 5352–5360.

[15] Chirino, A.J., Lous, E.J., Huber, M., Allen, J.P., Schenck, C.C., Paddock, M.L., Feher, G., and Rees, D.C. (1994) Crystallographic analyses of site-directed mutants of the photosynthetic reaction center from *Rhodobacter sphaeroides*. *Biochemistry*, **33**(15), 4584–4593.

[16] Cogdell, R.J., Gall, A., and Köhler, J. (2006) The architecture and function of the light-harvesting apparatus of purple bacteria: from single molecules to *in vivo* membranes. *Q. Rev. Biophys.*, **39**(03), 227–324.

[17] Deisenhofer, J., Epp, O., Miki, K., Huber, R., and Michel, H. (1985) Structure of the protein subunits in the photosynthetic reaction centre of Rhodopseudomonas viridis at 3 Å resolution. *Nature*, **318**, 618–624.

[18] Drews, G. and Golecki, J.R. (1995) Structure, molecular organization, and biosynthesis of membranes of purple bacteria. In *Anoxygenic Photosynthetic Bacteria*, pp. 231–257. Springer.

[19] Emsley, P. and Cowtan, K. (2004) *Coot*: model-building tools for molecular graphics. *Acta Crystallogr., Sect. D: Biol. Crystallogr.*, **60**(12), 2126–2132. doi: 10.1107/S0907444904019158.

[20] Ermler, U., Fritzsch, G., Buchanan, S.K., and Michel, H. (1994) Structure of the photosynthetic reaction centre from *Rhodobacter sphaeroides* at 2.65 Å resolution: cofactors and protein-cofactor interactions. *Structure*, **2**(10), 925 – 936. doi:http://dx.doi.org/10.1016/S0969-2126(94)00094-8.

[21] Fiedor, L., Kania, A., Mysliwa-Kurdziel, B., Orzel, L., and Stochel, G. (2008) Understanding chlorophylls: central magnesium ion and phytyl as structural determinants. *Biochim. Biophys. Acta, Bioenerg.*, **1777**(12), 1491–1500.

[22] Franken, E.M., Shkuropatov, A.Y., Francke, C., Neerken, S., Gast, P., Shuvalov, V.A., Hoff, A.J., and Aartsma, T.J. (1997) Reaction centers of *Rhodobacter*

sphaeroides R-26 with selective replacement of bacteriopheophytin by pheophytin *a*: I. Characterisation of steady-state absorbance and circular dichroism, and of the P^+ Q_A^- state. *Biochim. Biophys. Acta, Bioenerg.*, **1319**(2), 242–250.

[23] Frolov, D., Marsh, M., Crouch, L.I., Fyfe, P.K., Robert, B., van Grondelle, R., Hadfield, A., and Jones, M.R. (2010) Structural and spectroscopic consequences of hexacoordination of a bacteriochlorophyll cofactor in the *Rhodobacter sphaeroides* reaction center. *Biochemistry*, **49**(9), 1882–1892.

[24] Fyfe, P.K., Isaacs, N.W., Cogdell, R.J., and Jones, M.R. (2004) Disruption of a specific molecular interaction with a bound lipid affects the thermal stability of the purple bacterial reaction centre. *Biochim. Biophys. Acta, Bioenerg.*, **1608**(1), 11–22.

[25] Gabrielsen, M., Gardiner, A.T., and Cogdell, R.J. (2009) Peripheral complexes of purple bacteria. In *The Purple Phototrophic Bacteria*, pp. 135–153. Springer.

[26] Goldsmith, J.O. and Boxer, S.G. (1996) Rapid isolation of bacterial photosynthetic reaction centers with an engineered poly-histidine tag. *Biochim. Biophys. Acta, Bioenerg.*, **1276**(3), 171–175.

[27] Goldsmith, J.O., King, B., and Boxer, S.G. (1996) Mg coordination by amino acid side chains is not required for assembly and function of the special pair in bacterial photosynthetic reaction centers. *Biochemistry*, **35**(7), 2421–2428.

[28] Hanson, L.K. (1988) Theoretical calculations of photosynthetic pigments. *Photochem. Photobiol.*, **47**(6), 903–921.

[29] Heller, B.A., Holten, D., and Kirmaier, C. (1995) Characterization of bacterial reaction centers having mutations of aromatic residues in the binding site of the bacteriopheophytin intermediary electron carrier. *Biochemistry*, **34**(15), 5294–5302.

[30] Ignatov, N.V. and Litvin, F.F. (1994) Photoinduced formation of pheophytin/chlorophyll-containing complexes during the greening of plant leaves. *Photosynth. Res.*, **42**(1), 27–35.

[31] Imhoff, J.F. (1995) Taxonomy and physiology of phototrophic purple bacteria and green sulfur bacteria. In *Anoxygenic Photosynthetic Bacteria*, pp. 1–15. Springer.

[32] Jaschke, P.R. and Beatty, J.T. (2007) The photosystem of *Rhodobacter sphaeroides* assembles with zinc bacteriochlorophyll in a bchd (magnesium chelatase) mutant. *Biochemistry*, **46**(43), 12491–12500. doi:10.1021/bi701407k. PMID: 17910480.

[33] Jaschke, P.R., Hardjasa, A., Digby, E.L., Hunter, C.N., and Beatty, J.T. (2011) A *bchD* (magnesium chelatase) mutant of *Rhodobacter sphaeroides* synthesizes zinc bacteriochlorophyll through novel zinc-containing intermediates. *J. Biol. Chem.*, **286**(23), 20313–20322. doi:10.1074/jbc.M110.212605.

[34] Johansson, L.C., Wöhri, A.B., Katona, G., Engström, S., and Neutze, R. (2009) Membrane protein crystallization from lipidic phases. *Curr. Opin. Struct. Biol.*, **19**(4), 372–378. doi:10.1016/j.sbi.2009.05.006.

[35] Jones, M.R. (2008) Structural plasticity of reaction centers from purple bacteria. In *The Purple Phototrophic Bacteria*, pp. 295–321. Springer.

[36] Jones, M.R., Fyfe, P.K., Roszak, A.W., Isaacs, N.W., and Cogdell, R.J. (2002) Protein-lipid interactions in the purple bacterial reaction centre. *Biochim. Biophys. Acta, Biomembr.*, **1565**(2), 206–214.

[37] Jones, M.R., Visschers, R.W., Van Grondelle, R., and Hunter, C.N. (1992) Construction and characterization of a mutant of *Rhodobacter sphaeroides* with the reaction center as the sole pigment-protein complex. *Biochemistry*, **31**(18), 4458–4465. doi: 10.1021/bi00133a011.

[38] Kabsch, W. (2010) Integration, scaling, space-group assignment and post-refinement. *Acta Crystallogr., Sect. D: Biol. Crystallogr.*, **66**(2), 133–144.

[39] Katona, G. (2003) Lipidic Cubic Phase Crystal Structure of the Photosynthetic Reaction Centre from Rhodobacter sphaeroides at 2.35 ÅResolution. *J. Mol. Biol.*, **331**(3), 681–692. doi:10.1016/S0022-2836(03)00751-4.

[40] Katz, J., Strain, H., Harkness, A., Studier, M., Svec, W., Janson, T., and Cope, B. (1972) Esterifying alcohols in the chlorophylls of purple photosynthetic bacteria. A new chlorophyll, bacteriochlorophyll (gg), *all-trans*-geranylgeranyl bacteriochlorophyllide a. *J. Am. Chem. Soc.*, **94**(22), 7938–7939.

[41] Kirmaier, C., Gaul, D., DeBey, R., Holten, D., and Schenck, C.C. (1991) Charge separation in a reaction center incorporating bacteriochlorophyll for photoactive bacteriopheophytin. *Science*, **251**(4996), 922–927.

[42] Kirmaier, C., Holten, D., Bylina, E.J., and Youvan, D.C. (1988) Electron transfer in a genetically modified bacterial reaction center containing a heterodimer. *Proc. Natl. Acad. Sci. U.S.A.*, **85**(20), 7562–7566.

[43] Leslie, A.G. and Powell, H.R. (2007) Processing diffraction data with mosflm. In *Evolving Methods for Macromolecular Crystallography*, pp. 41–51. Springer.

[44] Lilburn, T.G., Prince, R.C., and Beatty, J.T. (1995) Mutation of the Ser2 codon of the light-harvesting B870 alpha polypeptide of *Rhodobacter capsulatus* partially suppresses the pufX phenotype. *J. Bacteriol.*, **177**(16), 4593–4600.

[45] Lin, S., Jaschke, P.R., Wang, H., Paddock, M., Tufts, A., Allen, J.P., Rosell, F.I., Mauk, A.G., Woodbury, N.W., and Beatty, J.T. (2009) Electron transfer in the *Rhodobacter sphaeroides* reaction center assembled with zinc bacteriochlorophyll. *Proc. Natl. Acad. Sci. U.S.A.*, **106**(21), 8537–8542. doi:10.1073/pnas.0812719106.

[46] Madigan, M.T. and Jung, D.O. (2009) An overview of purple bacteria: systematics, physiology, and habitats. In *The Purple Phototrophic Bacteria*, pp. 1–15. Springer.

[47] McAuley, K.E., Fyfe, P.K., Cogdell, R.J., Isaacs, N.W., and Jones, M.R. (2000) X-ray crystal structure of the YM210W mutant reaction centre from *Rhodobacter sphaeroides*. *FEBS Lett.*, **467**(2-3), 285–290.

[48] McAuley, K.E., Fyfe, P.K., Ridge, J.P., Isaacs, N.W., Cogdell, R.J., and Jones, M.R. (1999) Structural details of an interaction between cardiolipin and an integral membrane protein. *Proc. Natl. Acad. Sci. U.S.A.*, **96**(26), 14706–14711.

[49] Meyer, M. and Scheer, H. (1995) Reaction centers of *Rhodobacter sphaeroides* R26 containing C-3 acetyl and vinyl (bacterio)pheophytins at sites $H_{A,B}$. *Photosynth. Res.*, **44**(1-2), 55–65. doi:10.1007/BF00018296.

[50] Murshudov, G.N., Vagin, A.A., and Dodson, E.J. (1997) Refinement of macromolecular structures by the maximum-likelihood method. *Acta Crystallogr., Sect. D: Biol. Crystallogr.*, **53**(3), 240–255.

[51] Neupane, B., Jaschke, P., Saer, R., Beatty, J.T., Reppert, M., and Jankowiak, R. (2012) Electron transfer in *Rhodobacter sphaeroides* reaction centers containing Zn-bacteriochlorophylls: a hole-burning study. *J. Phys. Chem. B*, **116**(10), 3457–3466. doi:10.1021/jp300304r.

[52] Olson, T., Williams, J., and Allen, J. (2014) The three-dimensional structures of bacterial reaction centers. *Photosynth. Res.*, **120**(1-2), 87–98.

[53] Otwinowski, Z. and Minor, W. (1997) Processing of X-ray diffraction data collected in oscillation mode. In J. Charles W. Carter (Ed.), *Macromolecular Crystallography Part A*, vol. 276 of *Methods Enzymol.*, pp. 307 – 326. Academic Press. doi:http://dx.doi.org/10.1016/S0076-6879(97)76066-X.

[54] Pan, J., Saer, R.G., Lin, S., Guo, Z., Beatty, J.T., and Woodbury, N.W. (2013) The protein environment of the bacteriopheophytin anion modulates charge separation and charge recombination in bacterial reaction centers. *J. Phys. Chem. B*, **117**(24), 7179–7189. doi:10.1021/jp400132k.

[55] Parson, W.W. and Warshel, A. (2009) Mechanism of charge separation in purple bacterial reaction centers. In *The Purple Phototrophic Bacteria*, pp. 355–377. Springer.

[56] Pawlowicz, N.P., van Grondelle, R., van Stokkum, I.H., Breton, J., Jones, M.R., and Groot, M.L. (2008) Identification of the first steps in charge separation in bacterial photosynthetic reaction centers of *Rhodobacter sphaeroides* by ultrafast mid-infrared spectroscopy: electron transfer and protein dynamics. *Biophys. J.*, **95**(3), 1268–1284.

[57] Qian, P., Bullough, P.A., and Hunter, C.N. (2008) Three-dimensional reconstruction of a membrane-bending complex: The RC-LH1-PufX core dimer of *Rhodobacter sphaeroides*. *J. Biol. Chem.*, **283**(20), 14002–14011.

[58] Roszak, A.W., Gardiner, A.T., Isaacs, N.W., and Cogdell, R.J. (2007) Brominated lipids identify lipid binding sites on the surface of the reaction center from *Rhodobacter sphaeroides*. *Biochemistry*, **46**(11), 2909–2916.

[59] Roth, M., Lewit-Bentley, A., Michel, H., Deisenhofer, J., Huber, R., and Oesterhelt, D. (1989) Detergent structure in crystals of a bacterial photosynthetic reaction centre. *Nature*, **340**, 659–662.

[60] Saer, R.G., Hardjasa, A., Rosell, F.I., Mauk, A.G., Murphy, M.E.P., and Beatty, J.T. (2013) The role of *Rhodobacter sphaeroides* photosynthetic reaction center residue M214 in the composition, absorbance properties, and conformations of H_A and B_A cofactors. *Biochemistry*, **52**(13), 2206–2217. doi:10.1021/bi400207m.

[61] Saer, R.G., Pan, J., Hardjasa, A., Lin, S., Rosell, F., Mauk, A.G., Woodbury, N.W., Murphy, M.E., and Beatty, J.T. (2014) Structural and kinetic properties

of *Rhodobacter sphaeroides* photosynthetic reaction centers containing exclusively Zn-coordinated bacteriochlorophyll as bacteriochlorin cofactors. *Biochim. Biophys. Acta, Bioenerg.*, **1837**(3), 366 – 374.

[62] Scheer, H. (2006) An overview of chlorophylls and bacteriochlorophylls: biochemistry, biophysics, functions and applications. In B. Grimm, R.J. Porra, W. Rüdiger, and H. Scheer (Eds.), *Chlorophylls and Bacteriochlorophylls*, vol. 25 of *Advances in Photosynthesis and Respiration*, pp. 1–26. Springer Netherlands. doi:10.1007/1-4020-4516-6_1.

[63] Scheer, H. and Hartwich, G. (1995) Bacterial reaction centers with modified tetrapyrrole chromophores. In *Anoxygenic Photosynthetic Bacteria*, pp. 649–663. Springer.

[64] Senge, M.O. and Smith, K.M. (1995) Biosynthesis and Structures of the Bacteriochlorophylls. In R.E. Blankenship, M.T. Madigan, and C.E. Bauer (Eds.), *Anoxygenic Photosynthetic Bacteria*, vol. 2 of *Advances in Photosynthesis and Respiration*, pp. 137–151. Springer Netherlands. doi:10.1007/0-306-47954-0_8.

[65] Shioi, Y., Tomita, N., Tsuchiya, T., and Takamiya, K. (1996) Conversion of chlorophyllide to pheophorbide by Mg-dechelating substance in extracts of *Chenopodium album*. *Plant Physiol. Biochem.*, **34**(1), 41–47.

[66] Shochat, S., Arlt, T., Francke, C., Gast, P., van Noort, P.I., Otte, S.C., Schelvis, H.P., Schmidt, S., Vijgenboom, E., Vrieze, J., Zinth, W., and Hoff, A.J. (1994) Spectroscopic characterization of reaction centers of the (M)Y210W mutant of the photosynthetic bacterium *Rhodobacter sphaeroides*. *Photosynth. Res.*, **40**(1), 55–66.

[67] Struck, A. and Scheer, H. (1990) Modified reaction centers from *Rhodobacter sphaeroides* R26: exchange of monomeric bacteriochlorophyll with 132-hydroxybacteriochlorophyll. *FEBS Lett.*, **261**(2), 385–388.

[68] Sturgis, J.N. and Niederman, R.A. (2009) Organization and assembly of light-harvesting complexes in the purple bacterial membrane. In *The Purple Phototrophic Bacteria*, pp. 253–273. Springer.

[69] Vagin, A.A., Steiner, R.A., Lebedev, A.A., Potterton, L., McNicholas, S., Long, F., and Murshudov, G.N. (2004) REFMAC5 dictionary: organization of prior chemical knowledge and guidelines for its use. *Acta Crystallogr., Sect. D: Biol. Crystallogr.*, **60**(12), 2184–2195.

[70] Wakeham, M. and Jones, M. (2005) Rewiring photosynthesis: engineering wrong-way electron transfer in the purple bacterial reaction centre. *Biochem. Soc. Trans.*, **33**(4), 851–857.

[71] Watson, A.J., Fyfe, P.K., Frolov, D., Wakeham, M.C., Nabedryk, E., van Grondelle, R., Breton, J., and Jones, M.R. (2005) Replacement or exclusion of the B-branch bacteriopheophytin in the purple bacterial reaction centre: the H_B cofactor is not required for assembly or core function of the *Rhodobacter sphaeroides* complex. *Biochim. Biophys. Acta*, **1710**(1), 34–46.

[72] Wen, J., Harada, J., Buyle, K., Yuan, K., Tamiaki, H., Oh-oka, H., Loomis, R.A., and Blankenship, R.E. (2010) Characterization of an FMO variant of *Chlorobaculum tepidum* carrying bacteriochlorophyll *a* esterified by geranylgeraniol. *Biochemistry*, **49**(26), 5455–5463.

[73] Williams, J.C. and Allen, J.P. (2009) Directed modification of reaction centers from purple bacteria. In *The Purple Phototrophic Bacteria*, pp. 337–353. Springer.

[74] Willows, R.D. and Kriegel, A.M. (2009) Biosynthesis of bacteriochlorophylls in purple bacteria. In *The Purple Phototrophic Bacteria*, pp. 57–79. Springer.

[75] Winn, M.D., Ballard, C.C., Cowtan, K.D., Dodson, E.J., Emsley, P., Evans, P.R., Keegan, R.M., Krissinel, E.B., Leslie, A.G.W., McCoy, A., McNicholas, S.J.,

Murshudov, G.N., Pannu, N.S., Potterton, E.A., Powell, H.R., Read, R.J., Vagin, A., and Wilson, K.S. (2011) Overview of the *CCP*4 suite and current developments. *Acta Crystallogr., Sect. D: Biol. Crystallogr.*, **67**(4), 235–242. doi: 10.1107/S0907444910045749.

[76] Woodbury, N.W. and Allen, J.P. (1995) The pathway, kinetics and thermodynamics of electron transfer in wild type and mutant reaction centers of purple nonsulfur bacteria. In *Anoxygenic Photosynthetic Bacteria*, pp. 527–557. Springer.

[77] Wraight, C.A. and Gunner, M.R. (2009) The acceptor quinones of purple photosynthetic bacteria structure and spectroscopy. In *The Purple Phototrophic Bacteria*, pp. 379–405. Springer.

[78] Yeates, T., Komiya, H., Chirino, A., Rees, D., Allen, J., and Feher, G. (1988) Structure of the reaction center from *Rhodobacter sphaeroides* R-26 and 2.4.1: protein-cofactor (bacteriochlorophyll, bacteriopheophytin, and carotenoid) interactions. *Proc. Natl. Acad. Sci. U.S.A.*, **85**(21), 7993–7997.